Optimal Power Flow With Emerged Technologies of Voltage Source Converter Stations in Meshed Power Systems

EHAB E. ELATTAR[1,2]**, (Senior Member, IEEE), ABDULLAH M. SHAHEEN**[3]**,**
ABDALLAH M. ELSAYED[4]**, AND RAGAB A. EL-SEHIEMY**[5]**, (Senior Member, IEEE)**
[1]Electrical Engineering Department, College of Engineering, Taif University, Taif 21974, Saudi Arabia
[2]Electrical Engineering Department, Faculty of Engineering, Menoufia University, Shebin El-Kom 32511, Egypt
[3]Electrical Engineering Department, Faculty of Engineering, Suez University, Suez 43533, Egypt
[4]Electrical Engineering Department, Faculty of Engineering, Damietta University, Damietta 34517, Egypt
[5]Electrical Engineering Department, Faculty of Engineering, Kafrelsheikh University, Kafrelsheikh 33516, Egypt
Corresponding author: Ragab A. El-Sehiemy (elsehiemy@eng.kfs.edu.eg)

ABSTRACT It is no doubt that the optimal power flow (OPF) has great importance in electric power systems. It aims at assigning the adequate operating levels in order to meet the required demands with the objective of minimizing combined economic and environmental concerns. Integration of emerged technologies of voltage source converter (VSC) stations in AC meshed power systems changes foremost their corresponding operation and control features. The VSC stations are usually connected with each other through HVDC lines and consequently a multi-terminal direct current (MDC) system is established. This paper presents an improved manta ray foraging optimizer (IMRFO) for solving the OPF in electric power systems with and without emerged technologies of VSC stations. The proposed IMRFO aims at minimizing the total fuel costs, the total environmental emissions, and the total electrical losses. The MRFO simulates the foraging behaviors of the manta rays. MRFO is improved to handle multi-objectives by incorporating an outward store for the non-dominated Pareto individuals. The form of the fitness function is adaptively varied by iteratively changing their weights. Furthermore, a technique for order preference by similarity to ideal solution (TOPSIS) is applied to extract a suitable operating point among the resulted Pareto set. Several applications of the proposed IMRFO are presented for conventional IEEE 30-bus system, as an AC meshed power system, and modified IEEE 30-bus with emerged VSC stations, as a hybrid AC/MDC meshed power system. Simulation results declare that the proposed algorithm has great effectiveness and robustness features compared to the others. Also, various well-distributed Pareto solutions are obtained based on the proposed algorithm with adequate techno-economic-environmental characteristics.

INDEX TERMS Optimal power flow, AC/MDC meshed power system, VSC stations, manta ray foraging optimizer.

I. INTRODUCTION

The optimal power flow (OPF) problem is considered one of the old and modern studies. As 60 years ago after studying the OPF problem by Carpentier [1], the OPF problem still receives considerable attention because of the challenging nature of the problem and its important role in power system planning and operation. OPF aims at assigning the most adequate values of generators output powers, generators voltages, transformers tap settings, outputs of VAr compensators, FACTS parameters and setting, and other parameter of newly connected devices to minimize the predefined objective

The associate editor coordinating the review of this manuscript and approving it for publication was Ali Raza.

functions while satisfying the operating system constraints. OPF searches for the combined economic and environmental operation of electrical power systems by finding the effective operating points of the power systems, which can overcome previous problems satisfactorily. This optimal condition is distinct with respect to objective functions reducing generation costs, increasing system loadability, reducing transmission losses, reducing environmental emissions, improving voltage performance, and improving system reliability and security while maintaining different equality and inequality constraints [2].

Although many modern optimization methods have been applied to the OPF problem, including general nonlinear optimization techniques, interior point methods,

and meta-heuristic optimization methods [3], challenges remain for power systems operators and planners due to the continuous changes in electrical power systems. Integrated multi-terminal high voltage direct current transmission MTHVDC grids with AC networks changes the operation and control strategies of conventional grids [4]. Classical operation methodologies of power systems such as the economic dispatch, state estimation and optimal power flow, etc. need to be modified and adapted to this new context of integrated MTHVDC grids. Due to the importance of the OPF in operational and grid expansion planning as well as economic studies, OPF necessitates structural and formation changes to accommodate large-scale hybrid AC/DC power systems [5].

Nowadays, the capability of decoupled control of active and reactive power of the VSC enables the control of injected/absorbed reactive power to/from connected AC grids accordingly voltage control of AC side. As well, the VSC technology can controls the active and reactive power at the same time at each terminal independent of the DC power transmission. Modular Multilevel Converters (MMC) enables parallel connection of VSCs, which allows to form a Multi terminal high voltage direct current grids [6]. These merits increase the expand opportunities of integrated AC/MDC systems. Zhangbei project is the first meshed HVDC grid worldwide is designed in China to integrate massive amounts of renewable power in the heavily populated area around Beijing, being capable of supplying around 9 million people with clean energy. The first phase of this project, 4 terminals in a ring connection are planned, with 2 more coming in the second phase with a 648 km length of DC-grid [7]. Different HVDC transmission projects are under planning and execution worldwide [8]. Champa-Kurukshetra ultra HVDC project in India is completed with a 1305 km transmission link which can transmit 4.5 GW of electricity. This project will enable transmitting electricity from power generating plants located across the state of Chhattisgarh to a GE-built rectifier station in Champa [9]. Nelson River HVDC transmission system in Manitoba is the backbone of power supply to southern Manitoba from the northern hydroelectric generating stations on the Nelson River. In that project, bipole 1 has a rating of 1854 MW at ±463kV and transmits the power from the northern terminal at Radisson Station over approximately 900 km to the Dorsey terminal near Winnipeg. Bipole 2 has a rating of 2000 MW at ±500 kV and transmits the power to approximately 40 km [10]. The Egyptian/Saudi electrical interconnection project aims to exchange a capacity of 3000 MW between the two countries using HVDC bipolar transmission technology on 500 kV through one substation in Egypt and two substations in Medina & Tabuk in KSA with overhead lines on both and a submarine cable crossing the Gulf of Aqaba [11].

Different grid technologies of MDC grids are possible: shore-to-shore, radial, meshed, cluster with multi way interconnectors, and a combination of interconnectors, amongst others. Growing penetration of offshore wind and ocean energy includes wave, tidal current, tidal range, osmotic, and ocean thermal energies are expected to have higher power soon [12]. This requires increased reliance on power transmission with HVDC to reduce the investment costs [13]. Voltage regulation capability of the VSC enhances the performance of connected AC grid by generating or consuming reactive power. A predefined power flow along a certain transmission cable can be quickly achieved using the VSC based HVDC. Then, MDC grids can achieve the needed reliability, flexibility and controllability to meet the main grid code requirements such as the operating frequency range, active and reactive power control, support during voltage dips, and fault ride-through capabilities [14].

One of the adopted solutions of the increased consumer demand over the capability limits of the ageing power grids and increased penetration of non-dispatchable renewable sources is the optimal power flow (OPF). OPF aims at assigning the most adequate values of generators output powers, generators voltages, transformers tap settings, outputs of VAr compensators, FACTS parameters and setting, and other parameter of newly connected devices to minimize the predefined objective functions while satisfying the operating system constraints. OPF searches for the combined economic and environmental operation of the electrical power systems by searching for the effective operating points of the power systems, which can overcome previous problems satisfactorily. This optimal condition is distinct with respect to objective functions reducing generation costs, increasing system loadability, reducing transmission losses, reducing environmental emissions, improving voltage performance, and improving system reliability and security while maintaining the different equality and inequality constraints [2], [15].

Integration of HVDC grids with AC networks changes the operation and control strategies of conventional grids. Classical operation methodologies of power systems such as the economic dispatch [16], state estimation [17] and optimal power flow [18], etc. need to be modified and adapted to this new context of integrated MDC grids. Due to the importance of the OPF in operational and grid expansion planning as well as economic studies, OPF necessitates structural and formation changes to accommodate large-scale hybrid AC/DC power systems. The OPF problem becomes even more nonlinear, non-convex and complex problem when applied to integrated AC/MDC systems where it involves many optimization variables and system constraints [19]. Several literatures dealt with OPF either for separate AC networks [20], [21] or separate DC grids [22], [23]. Lately, mathematical formulation of OPF for AC/MDC networks got a great attention in literatures such as [5], [24]–[27]. The assessment of VSC-HVDC systems in a lot of these papers were limited to two-terminal configuration. While, the embedded of meshed DC grids into an AC grid increases the complexity of operation and control analysis of such systems [24], [28]. A few researchers ignore the modelling of some elements of AC/MDC to simplify the problem such as neglecting the DC power-flow equations [29]. Although, the VSC systems

have been included into power flow calculation of a hybrid AC/MDC systems in many previous literatures as mentioned earlier, but fewer literatures consider VSC systems under an optimization context. Peñalbaa *et al.* [4] solved the hybrid network using the second-order cone programming (SOCP) technique. Cao *et al.* [30] applied the Primal-Dual Interior Point (PDIP) algorithm as well as modified Jacobian and Hessian matrices. Feng *et al.* [24] solved this problem using the Interior Point Optimizer (IPOPT) to seek solutions for the non-linear model built in General Algebraic Modelling System. Zhao *et al.* [26] introduced an extended OPF model to consider loss modelling of different converter operation modes. In those papers, the effect of transformer-tap settings and VAr compensation in AC grid were ignored whilst the utilized tools are based on the initial starting point with some simplifications that reduces the required accuracy.

Manta Ray Foraging Optimizer (MRFO) is a recent optimization algorithm that is designed for handling real-valued optimization applications. It has been firstly proposed by Zhao *et al.* [31], and it is inspired based on the intelligent and unique strategies of the manta rays in their foraging the plankton. In [31], its performance is assessed with itemized comparisons with other recent optimizers in optimizing several benchmark and real-world engineering design functions. In [32], a successful attempt of applying the MRFO has been carried out for extracting the electrical parameters of proton exchange membrane fuel cells.

In this paper, an improved manta ray foraging optimizer (IMRFO) to solving the OPF in electric power systems with and without emerged technologies of VSC stations. It is improved to handle multi-objectives by incorporating an outward store for the non-dominated Pareto individuals. The form of the fitness function is adaptively varied by iteratively changing their weights. Furthermore, a technique for order preference by similarity to ideal solution (TOPSIS) is applied to extract one of the Pareto set as a suitable operating point. Several applications of the proposed IMRFO are presented for conventional IEEE 30-bus system, as an AC meshed power system, and modified IEEE 30-bus with emerged VSC stations, as a hybrid AC/MDC meshed power system. find the optimal operation of hybrid AC/MDC grid. For these applications, a comparative analysis is executed between the proposed algorithm and several recent algorithms. The main contribution of this paper can be summarized as follow:

➢ A new IMRFO is presented for solving the OPF in electric power systems with and without emerged technologies of VSC stations.
➢ A dynamic adaptation to the fitness function is extended to the IMRFO based on varying the shape of the fitness in each iteration. Furthermore, a TOPSIS is applied to select the final candidate operating point of the hybrid AC/MDC power transmission systems.
➢ The proposed multi-dimensional framework aims at minimizing the total fuel costs, the environmental emissions of the generation units and the total losses over the AC, MDC transmission lines and VSCs stations.

➢ Effectiveness of the proposed technique has been checked with detailed assessment with other recent techniques in terms of its solution quality and robustness
➢ Simulation results show the capability of the proposed method in finding well distributed Pareto solutions with preferable operating technical and economic concerns.

The rest sections of this work present the following: Section 2 shows the principle of the optimal operation of hybrid grids. Section 3 shows the optimal IMRFO based operation procedure. Section 4 reports the simulation results for three hybrid AC/MDC grids. Section 5 concludes the salient findings.

II. OPF IN CONVENTIONAL AC POWER SYSTEMS
A. OPF OBJECTIVES
The OPF problem mathematical model in conventional power systems is generally formulated as follows:

$$\text{Min OF} = \{F_1(x,y), F_2(x,y)....,F_M(x,y)\} \quad (1)$$
$$\text{Subject to: } g(x,y) = 0 \quad (2)$$
$$h(x,y) \leq 0 \quad (3)$$

where, OF is the vector of M objective functions; x and y are the decision and dependent variables, respectively. Therefore, the OPF is a nonlinear, multimodal, and multi-objective optimization problem for minimizing the fuel generation costs (FGC) and the total environmental emissions (TEE) of the generation stations. Besides that, the total transmission losses are considered. The FGC are modeled considering the multiple ripples that are accompanied to the valve point loading effect, as in practical power system. Thus, the fuel generation costs can be modeled as rectified sinusoids added to the polynomial quadratic costs and it is expressed as follows as:

$$\text{FGC} = \sum_{i=1}^{N_g} a_i Pg_i^2 + b_i Pg_i + c_i + \left| e_i(\sin f_i(Pg_{i,min} - Pg_i)) \right| \quad (4)$$

where, Pg_i is the MW active power output of each generator i; a_i, b_i, and c_i are the corresponding cost coefficients; $Pg_{i,min}$ is the lower limit of the active power output; e_i, and f_i are the valve point loading coefficients.

In power systems, the fossil-fueled generators are the main source of the atmospheric pollutants where sulphur oxides (Sox), nitrogen oxides (NOx) and second carbon oxide (CO2) are emitted. The total environmental emissions (TEE) in ton/hr of these pollutants can be modeled as the summation of quadratic and exponential function in terms of the output power as follows:

$$\text{TEE} = \sum_{i=1}^{N_g} (\gamma_i Pg_i^2 + \beta_i Pg_i + \alpha_i)/100 + \zeta_i e^{\lambda_i Pg_i} \quad (5)$$

where γ_i, β_i, α_i, ξ_i, and λ_i are the emission coefficients of the atmospheric pollutants.

Also, the total transmission losses in AC power systems is another objective to be minimized as:

$$TTL_{AC} = \sum_{i,j \in N_{AC,b}} G_{ij} \left(V_i^2 + V_j^2 - 2V_i V_j \cos\theta_{ij} \right) \quad (6)$$

B. OPF CONSTRAINTS IN AC POWER SYSTEMS

For the OPF problem in AC power systems, the decision variables are the power outputs of the generators (Pg_1, Pg_2, ... Pg_{Ng}), its voltages (Vg_1, Vg_2, ..., Vg_{Ng}), VAR injection of the reactive power sources (Qc_1, Qc_2, ..., Qc_{Nq}), and transformer tap settings (Tap_1, Tap_2, ..., Tap_{Nt}) where, Ng, Nq, and Nt are the number of generators, the number of the VAR sources, and the number of tap changing transformers, respectively. On contrary, the dependent variables are load voltage magnitudes (VL_1, ..., VL_{NPQ}), VAR outputs of the generators (Qg_1, Qg_2, ..., Qg_{Ng}), and transmission line power flow (SF_1, ..., SF_{NF}) where, NPQ and NF are the number of load buses and lines, respectively.

Firstly, the equality constraints of the load flow balance equations must be maintained as follows:

$$Qg_i - QL_i + Qc_i - V_i \sum_{j=1}^{N_b} V_j(G_{ij}\sin\theta_{ij} - B_{ij}\cos\theta_{ij}) = 0,$$
$$i = 1,2, \ldots NPQ \quad (7)$$

$$Pg_i - PL_i - V_i \sum_{j=1}^{N_b} V_j(G_{ij}\cos\theta_{ij} + B_{ij}\sin\theta_{ij}) = 0,$$
$$i = 1, \ldots N_b - slack \quad (8)$$

where, N_b is the number of buses; PL and QL are the active and reactive power demand, respectively; G_{ij} and B_{ij} are mutual conductance and susceptance between bus i and j, respectively.

Secondly, the operational variables have to be satisfied within the corresponding constraints as follows [33], [34]:

$$Pg_i^{min} \leq Pg_i \leq Pg_i^{max}, \quad i = 1, 2, \ldots\ldots Ng \quad (9)$$
$$Vg_i^{min} \leq Vg_i \leq Vg_i^{max}, \quad i = 1, 2, \ldots\ldots Ng \quad (10)$$
$$Qg_i^{min} \leq Qg_i \leq Qg_i^{max}, \quad i = 1, 2, \ldots\ldots Ng \quad (11)$$
$$Tap_k^{min} \leq Tap_k \leq Tap_k^{max}, \quad k = 1, 2, \ldots\ldots Nt \quad (12)$$
$$Qc_q^{max} \leq Qc_q \leq Qc_q^{max}, \quad q = 1, 2, \ldots\ldots Nq \quad (13)$$
$$V_{L_i}^{min} \leq V_{L_i} \leq V_{L_i}^{max}, \quad i = 1, 2, \ldots\ldots NPQ \quad (14)$$
$$|S_F| \leq S_F^{max}, \quad L = 1, 2, \ldots\ldots Nf \quad (15)$$

where the superscripts "min" and "max" indicate the minimum and maximum limits of the related variable.

III. OPTIMAL POWER FLOW IN HYBRID AC/MDC POWER SYSTEMS

A. VSCS MODEL IN AC/MDC POWER SYSTEM

The equivalent circuit of a VSC station is illustrated in Fig. 1. As shown, the VSC is modeled as a controlled voltage source (Vc_i) that is connected to the AC system buses via its phase
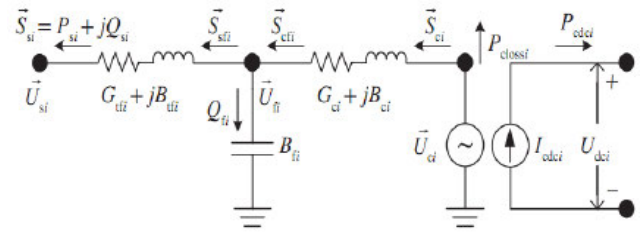

FIGURE 1. Equivalent circuit of the VSC station [35].

reactor and transformer which have equivalent impedance ($R_{ik}+jX_{ik}$). Vs_k refers to the bus voltage at AC system. Thus, the injected MVA (S_{ki}) into VSCs from the AC system is given by:

$$S_{ki} = P_{ki} + jQ_{ki} = Vs_k I_{ki}^*, i = 1 \ldots N_{VSC}, \quad k = 1 \ldots N_{ac} \quad (16)$$

where, P and Q are the injected active and reactive power, respectively. N_{VSC} and N_{ac} are the number of VSCs and the connected AC buses, respectively. I_{ki} is the corresponding injected current which can be calculated as:

$$I_{ki} = \frac{Vs_k - Vc_i}{R_{ik} + jX_{ik}} \quad (17)$$

From (1) and (2); the active and reactive power at each converter side (Pc_i+jQc_i) and the corresponding AC connected side (Ps_k+jQs_k) can be represented as:

$$Pc_i = -Vc_i^2 G_{ik} + Vs_k Vc_i[G_{ik}\cos(\theta_{ki}) + B_{ik}\sin(\theta_{ki})] \quad (18)$$
$$Qc_i = -Vc_i^2 B_{ik} - Vs_k Vc_i[G_{ik}\sin(\theta_{ki}) + B_{ik}\cos(\theta_{ki})] \quad (19)$$
$$Ps_k = Vs_k^2 G_{ik} - Vs_k Vc_i[G_{ik}\cos(\theta_{ki}) + B_{ik}\sin(\theta_{ki})] \quad (20)$$
$$Qs_k = -Vs_k^2 B_{ik} - Vs_k Vc_i[G_{ik}\sin(\theta_{ki}) - B_{ik}\cos(\theta_{ki})] \quad (21)$$

where, G and B are the conductance and susceptance of the DC line, respectively; θ_{ki} is the phase angle difference between the VSC and the connected AC bus.

B. OPF FORMULATION IN HYBRID AC/MDC POWER SYSTEMS

In hybrid AC/MDC power systems, the OPF problem targets the similar multi-objective functions without jeopardizing the regarded constraints to both AC and MDC power transmission systems. It is handled as a multi-objective optimization problem for minimize the FGC, TEE and TLL. The TLL in hybrid AC/MDC power systems is formulated in Eq. (22) which are three parts incorporating the power losses in the AC power systems of Eq. (6), VSCs stations of Eq. (23), and MDC power systems of Eq. (24).

$$TLL = TLL_{AC} + TLL_{DC} + TLL_{VSC} \quad (22)$$
$$TLL_{DC} = \sum_{i,j \in N_{DC,b}} R_{ij} I_{ij}^2 \quad (23)$$
$$TLL_{VSC} = \sum_{i=1}^{N_{VSC}} \varphi_{1,i} I_{c,i}^2 + \varphi_{2,i} I_{c,i} + \varphi_{3,i} \quad (24)$$

where φ_1, φ_2, and φ_3 are the loss coefficients related to each VSC. As shown, the VSC losses is generalized in a quadratic formula with the injected VSC current (Ic_i) [36]:

1) DECISION AND DEPENDENT VARIABLES OF THE OPF IN HYBRID AC/MDC POWER SYSTEMS

In AC/MDC power systems, the decision variables can be classified into two categories. Firstly, the conventional controls in the AC grids which are previously mentioned in Section II.B. Secondly, the advanced control of the VSC type devices where there are four classes of the control strategies [36]:

1. V_{dc}-Q_c constant control: This mode provides constant voltage at DC side with constant reactive power at AC side.
2. V_{dc}-V_c constant control: This mode provides constant voltage at DC and AC sides.
3. P_{dc}-Q_c constant control: This mode provides constant active power transferred in the DC line with constant reactive power at AC side.
4. P_{dc}-V_c constant control: This mode provides constant active power transferred in the DC line with constant AC voltage.

Similarly, the dependent variables can be classified related to AC side and MDC side. For the AC side, the dependent variables are same as mentioned in Section II.B. For the MDC side, the dependent variables are the DC bus voltages and the power flow though the DC lines.

2) CONSTRAINTS OF THE OPF IN HYBRID AC/MDC POWER SYSTEMS

In addition to Eqs. (7 and 8), the DC system power flow must be considered as equality constraints as:

$$P_{dc,i} = V_{dc,i} \sum_{\substack{i=1 \\ i \neq j}}^{N_{VSC}} G_{dc,ij}(V_{dc,i} - V_{dc,j}) \qquad (25)$$

where, $P_{dc,i}$ is the injected power at bus i. Moreover, the operational variables for the DC systems, in addition to Eqs. (9 and 15), must be satisfied within the corresponding constraints as follows:

$$Ps_i^{min} \leq Ps_i \leq Ps_i^{max}, \quad i = 1, 2,\ldots\ldots N_{VSC} \qquad (26)$$

$$Qs_i^{min} \leq Qs_i \leq Qs_i^{max}, \quad i = 1, 2,\ldots\ldots N_{VSC} \qquad (27)$$

$$Vc_i^{min} \leq Vc_i \leq Vc_i^{max}, \quad i = 1, 2,\ldots\ldots N_{VSC} \qquad (28)$$

$$V_{dc,i}^{min} \leq V_{dc,i} \leq V_{dc,i}^{max}, \quad i = 1, 2, \ldots\ldots N_{DC} \qquad (29)$$

$$d_i^{min}/2 \leq \sqrt{(Ps_i - P_o)^2 - (Qs_i - Q_o)^2} \leq d_i^{max}/2,$$
$$i = 1, 2,\ldots\ldots N_{DC} \qquad (30)$$

where, (P_o, Q_o) is the circles centre related to the VSC PQ-capability curve with diameter of d. "min" and "max" superscripts indicate the minimum and maximum limits of their related variable. Eq. (30) represents the PQ capability curve of each VSC that must be maintained.

IV. PROPOSED IMRFO FOR OPF IN HYBRID AC/MDC POWER TRANSMISSION SYSTEMS

A. MRFO ALGORITHM

Manta Ray Foraging Optimizer (MRFO) is a recent algorithm [31], which is inspired from the intelligent and unique strategies of the marine manta rays in their foraging. It mimics three distinct individual foraging organizations of the manta rays. The first one is the chain foraging where some of the manta rays forage in a small cooperative way since they are organized in an orderly line to funnel the greatest quantity of plankton into their gills. The second is the cyclone foraging where many manta rays are linked up in a spiral shape to create a centralized spiraling peak. This forces the water up towards the surface and withdraws the plankton inside their mouths. The latter strategy is the somersault foraging. The manta rays search for the planktons' position and swim towards them. The manta rays indicate the individuals in the search space that seek for the minimum fitness which is the planktons' position.

The MRFO begins with initialization stage after identifying the population number (P_N) of the manta rays and the maximum number of iterations (M_{It}). Thus, the D-dimensional individuals (Y) can be initially created as:

$$Y_{m,n} = Y_n^{min} + r.(Y_n^{max} - Y_n^{min}) \quad \forall m \in P_N \ \& \ n \in D \quad (31)$$

where, $Y_{m,n}$ is the individual of each decision variable (n) of each manta ray (m); r indicates a random uniformly distributed number within range [0, 1]. The superscripts 'min' and 'max' refer to the bounds of the decision variables.

In the first strategy, which is the chain foraging, every individual is updated as follows:

$$Y_{m,n}^* = \begin{cases} Y_{m,n} + (Y_{B,n} - Y_{m,n})(r + \sigma) & \text{if } m = 1 \\ Y_{m,n} + r(Y_{m-1,n} - Y_{m,n}) + \sigma(Y_{B,n} - Y_{m,n}) \\ \forall m = 2{:}P_N \end{cases} \quad (32)$$

where, Y^* and Y are the new and old position of the manta ray at the following iteration. Y_B is the best position of the plankton food that has the highest concentration or fitness. σ is a weight coefficient that is varied each iteration as:

$$\sigma = 2.r.\sqrt{|\log(r)|} \qquad (33)$$

As shown, the new position of the manta ray is generated based on the best individual and the preceding one.

In the second strategy, which is the cyclone foraging, the iterations are equally divided into two parts. The first half focus on improving the exploration of the MRFO. Consequently, each individual is updated, in the first half of iterations, as follows:

$$Y_{m,n}^* = \begin{cases} Y_{R,n} + (Y_{R,n} - Y_{m,n})(r + \beta) & \text{if } m = 1 \\ Y_{R,n} + r(Y_{m-1,n} - Y_{m,n}) + \beta(Y_{R,n} - Y_{m,n}) \\ \forall m = 2{:}P_N \end{cases} \quad (34)$$

where, Y_R is a created individual in a random way within the considered bounds as follow:

$$Y_{R,n} = Y_n^{min} + r.(Y_n^{max} - Y_n^{min}) \quad \forall n \in D \qquad (35)$$

TABLE 1. Initial table for proposed topsis method.

Criteria	Losses	I_{fault}	FCL size	TVSI	TVD
Weight factor	w_1	w_2	w_3	w_4	w_5
Solution 1	X_{11}	X_{12}	X_{13}	X_{14}	X_{15}
⋮	⋮	⋮	⋮	⋮	⋮
Solution 100	X_{1001}	X_{1002}	X_{1003}	X_{1004}	X_{1005}

where, β is an adaptive weight coefficient which is varied by the following equation:

$$\beta = 2\, e^{r_1 \left(\frac{M_{It} - It + 1}{M_{It}} \right)} . \sin(2\pi r_1) \tag{36}$$

where, It is the current iteration and r_1 a random uniformly distributed number within range [0, 1]. The second half of the iterations focus on improving the exploitation of the MRFO. Regarding to that, each individual is updated as follows:

$$Y^*_{m,n} = \begin{cases} Y_{B,n} + (Y_{B,n} - Y_{m,n})(r + \beta) & \text{if } m = 1 \\ Y_{B,n} + r(Y_{m-1,n} - Y_{m,n}) + \beta(Y_{B,n} - Y_{m,n}) \\ \forall m = 2 : P_N \end{cases} \tag{37}$$

In the third strategy, which is the somersault foraging, the position of each manta ray is updated around the best extracted position as follows:

$$Y^*_{m,n} = Y_{m,n} + S(r_2 Y_{B,n} - r_3 Y_{m,n}) \quad \forall m \in P_N \ \& \ n \in D \tag{38}$$

where S is the somersault coefficient (S = 2) that controls the somersault domain of the manta rays and, r_2 and r_3 are random numbers within range [0, 1].

B. PROPOSED IMRFO FOR MULTI-OBJECTIVE OPF IN AC/MDC POWER SYSTEMS

In the MRFO, the new positions are generated based on the chain foraging strategy of Eq. (32), the cyclone foraging strategy of Eqs. (35 and 37), or the somersault foraging of Eq. (38). The MRFO is fundamentally sensitive to the best position of the plankton food. Therefore, the proposed IMRFO creates an adequate adaptation to the fitness function based on dynamic variation of the shape of the fitness in each iteration using dynamic weighting factor. Therefore, the objective function can be formulated as follows:

$$O = \sum_{i=1}^{M} \omega_i \frac{F_i}{F_i^{max}} \tag{39}$$

$$\omega_1 = \begin{cases} 1 & \text{if } It < M_{It}/3 \\ 1 - \dfrac{It}{M_{It}} & \text{else} \end{cases} \tag{40}$$

$$\omega_i = \frac{1 - \omega_1}{M}, \quad i = 2, 3, \dots M \tag{41}$$

where, ω_i is the weight factor related to each objective (i). Based on (40−41), the considered fitness function is dynamically changed in a single simulation operation which results
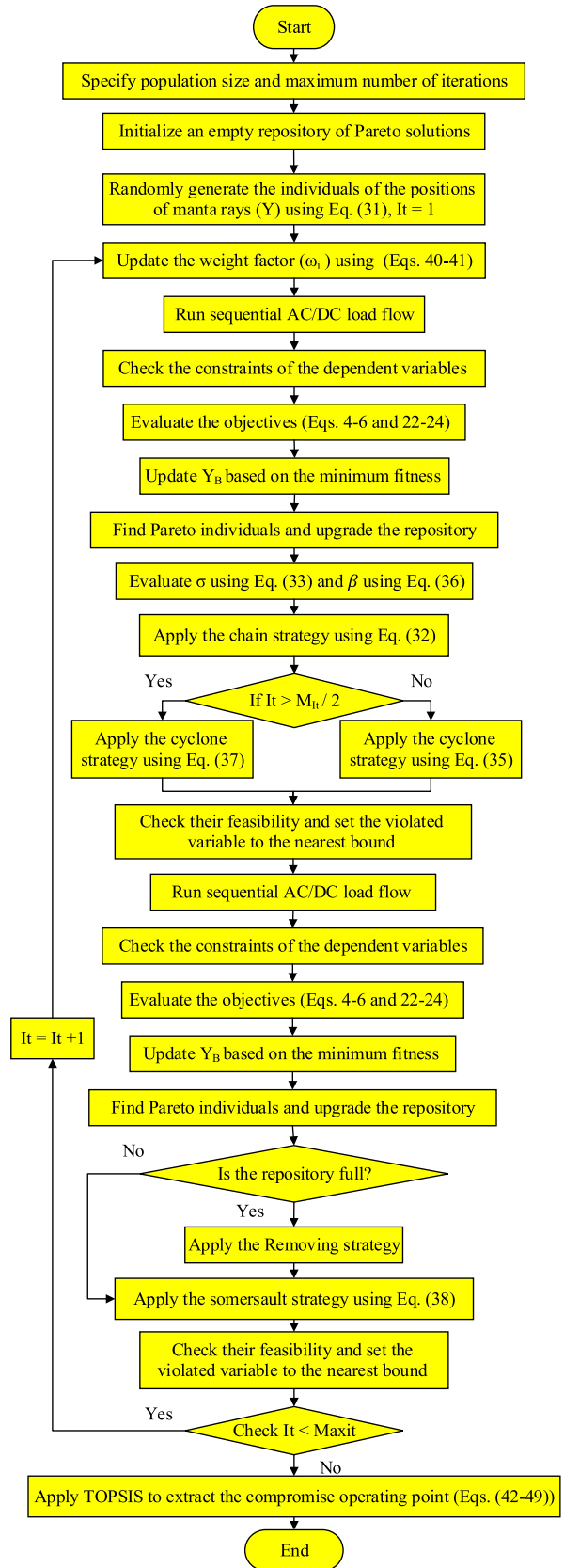

FIGURE 2. Proposed IMRFO for handling the multi-objective OPF.

TABLE 2. Simulation results for Case 1 of the IEEE 30-bus system.

Variables	Initial	Case 1A	Case 1B	Case 2	Case 3	Case 4	Case 5	Case 6
Pg_1	99.24	1.0999	1.1	1.0997	1.064	1.0965	1.0974	1.0902
Pg_2	80	1.0824	1.0879	1.0973	1.058	1.0835	1.0844	1.0639
Pg_5	50	1.0539	1.0603	1.0804	1.0369	1.0349	1.0657	1.047
Pg_8	20	1.0612	1.0692	1.0868	1.0463	1.0574	1.063	1.0358
Pg_{11}	20	1.0443	1.0732	1.0959	1.0289	1.0689	1.0235	1.0469
Pg_{13}	20	1.095	1.0877	1.0881	1.0457	1.0846	1.0577	1.0641
Vg_1	1.05	1.046	1.0416	1.0265	0.9975	0.9985	1.0858	0.9871
Vg_2	1.04	0.9515	0.9233	0.9456	1.0673	0.9887	0.9654	0.9864
Vg_5	1.01	1.0072	1.0126	0.9977	0.9914	1.0087	1.0133	1.0248
Vg_8	1.01	0.9579	0.9612	0.9782	0.9845	1.0016	0.9987	1.0035
Vg_{11}	1.05	23.2236	9.3548	1.837	23.9486	14.6879	11.1131	6.4946
Vg_{13}	1.05	22.1306	29.2171	14.9643	20.4206	13.0156	8.2954	11.3328
Tap_{6-9}	1.078	3.1176	2.4897	5.1244	3.436	6.1365	7.3777	6.732
Tap_{6-10}	1.069	6.0334	8.6216	6.7093	9.0436	7.1448	10.9175	7.5903
Tap_{4-12}	1.032	4.9365	3.2529	4.2202	4.2142	4.5553	4.9231	4.4355
Tap_{28-27}	1.068	11.5376	9.6476	9.6325	8.9709	9.4029	8.9028	18.2547
Qc_{10}	0	1.9733	1.9209	2.2354	2.4495	9.7873	2.5525	4.1599
Qc_{12}	0	5.0815	6.5779	6.2511	8.0489	3.2328	7.3442	10.3406
Qc_{15}	0	2.1158	2.1128	2.1304	3.256	5.9179	3.0361	3.7792
Qc_{17}	0	199.988	177.0137	51.5745	64.1786	153.9167	138.8643	134.9824
Qc_{20}	0	39.458	48.7911	79.7198	67.4283	64.1674	52.3006	63.0426
Qc_{21}	0	18.3151	21.2684	49.9809	49.9993	20.2242	25.6456	24.3908
Qc_{23}	0	12.4972	21.0819	34.99	34.9991	21.0968	34.35	32.7842
Qc_{24}	0	11.2494	11.7699	29.9862	29.997	16.5435	19.2133	16.6066
Qc_{29}	0	12.0001	12.0774	39.9945	39.9985	15.3862	19.3667	18.5032
FGC ($/hr)	975.64	830.6795	798.9888	1026.3	1015.3	849.1	855.0785	854.5635
TLL (MW)	5.596	10.1079	8.6025	2.846	3.2009	7.9348	6.3405	6.9098
TEE (ton/hr)	0.2390963	0.4418	0.366	0.2071	0.204754	0.305	0.2801	0.2777

TABLE 3. Comparisons for minimizing the FGC (Case 1A) for the IEEE 30-bus system.

Algorithm	Year of publication	FGC ($/hr)
Artificial bee colony (ABC) [42]	2013	800.66
Teaching-learning algorithm [42]	2015	800.4212
Differential evolution (DE) [41]	2016	799.0827
Symbiotic organisms search (SOS) [44]	2017	801.5733
Moth swarm algorithm (MSA) [45]	2017	800.5099
Developed grey wolf algorithm (DGWA) [46]	2018	800.433
Improved moth flame algorithm (IMFA) [46]	2019	800.3848
Grasshopper optimizer (GO) [48]	2020	800.9728
Adaptive grasshopper optimizer (AGO) [48]	2020	800.0212
Proposed IMRFO	2020	798.9888

TABLE 4. Comparisons for minimizing the TEE (Case 3) for the IEEE 30-bus system.

Algorithm	Year of publication	TEE (ton/hr)
Artificial bee colony (ABC) [42]	2013	0.204826
Krill herd algorithm (KHA) [49]	2018	0.2049
Stud krill herd algorithm (SKHA) [49]	2018	0.2048
Adaptive real coded biogeography-based optimization (ARBO) [50]	2015	0.2048
Teaching learning-based optimization (MTLBO) [51]	2015	0.205
Modified teaching learning-based optimization (MTLBO) [51]	2015	0.20493
Grasshopper optimizer (GO) [48]	2020	0.20492
Adaptive grasshopper optimizer (AGO) [48]	2020	0.20484
Proposed IMRFO	2020	0.204754

in high diversity in the individuals with high intensifications on an adaptive normalized goal. The normalization process that is integrated with the weights variation results in equal handling of the various objectives.

For creating Pareto individuals, the proposed IMRFO is evolved incorporating an external repository to store the non-dominated solutions and so Pareto dominance is utilized to update this repository. In each iteration, the updated individuals are compared to existed Pareto solutions in the repository to exclude the dominated solutions. Consequently, it is updated and if it is fulfilled, a removing strategy is applied by deleting some of the Pareto candidates in the most crowded areas via roulette wheel selection [37].

For handling the OPF problem, the balance equations in AC power system of Eqs. (7 and 8) and in MDC power

system of Eq. (25) are guaranteed inherently via sequential AC/DC power flow method [38]. For the operational limits of the decision variables, they are started satisfying their bounds and if any of them is violated during the iterations, it is randomly re-generated within the following appropriate range. For the operational limits of the dependent variables in AC/MDC power transmission systems, they are augmented in the considered objective functions using quadratic penalty terms. On this basis, the solution, which causes any violation in the constraints of the dependent variables, couldn't be selected in the next iteration. Thus, each new position is compared to its equivalent in preceding iteration in terms of the attained objectives. The new position substitutes the prior one
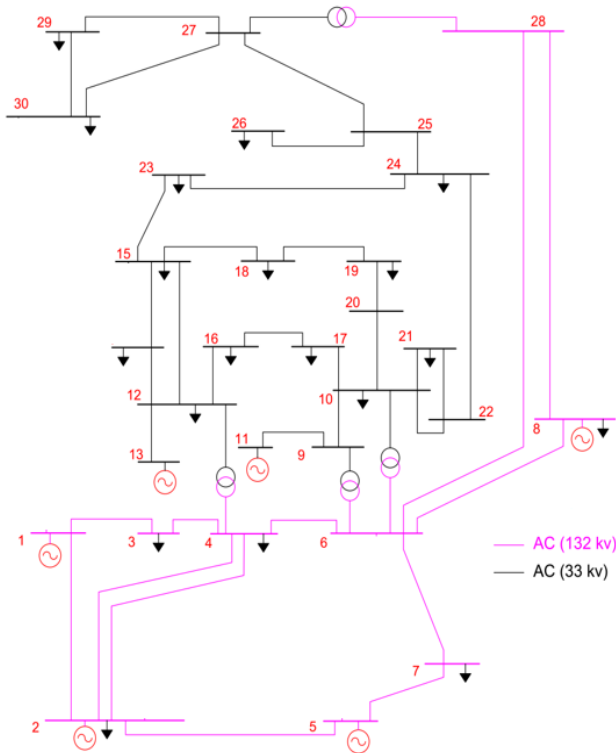
FIGURE 3. IEEE 30-bus system.

FIGURE 4. Convergence curve of the proposed algorithm for a. FGC Minimization, b. TLL Minimization, and c. Minimization of the TEE.
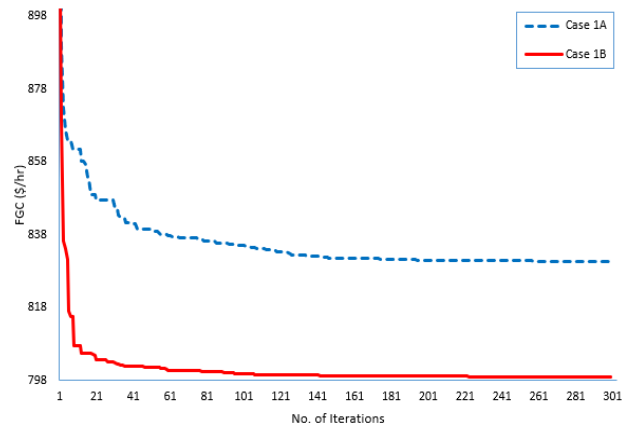
if the new position doesn't be dominated by it. This method preserves the diversity and ameliorates the solution quality. Therefore, a set of pareto optimal solutions is generated and stored. Fig. 2 depicts the flowchart of the proposed IMRFO for optimal operation of for OPF in hybrid AC/MDC power systems.

To extract the compromise operating point, a technique for order preference by similarity to ideal solution (TOPSIS) is implemented to select a compromise solution to achieve the operator requirements. TOPSIS is a technique to choose the optimal alternative (A) from multi alternatives with multi criteria (X) [39]. Table 1 shows the initial table for proposed TOPSIS method. In table, the alternatives are the hundred optimal solutions that are stored in the archive while each of criteria is represented by one of the OFs as follow:-
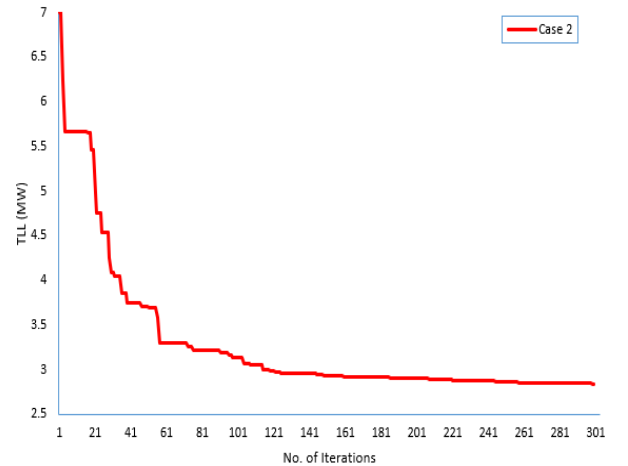
$$X_{ij} = \begin{bmatrix} x_{11} & x_{12} & \cdots\cdots & x_{15} \\ x_{21} & x_{21} & \cdots\cdots & x_{21} \\ \vdots & \vdots & \ddots & \vdots \\ x_{1001} & x_{1002} & \cdots & x_{1005} \end{bmatrix} \quad (42)$$

where, X_{ij} is the alternative for each Pareto solution (i) and regarded criteria (j). As each of criteria has a different measuring unit, each alternative is represented by a set of normalized parameter value as follow:
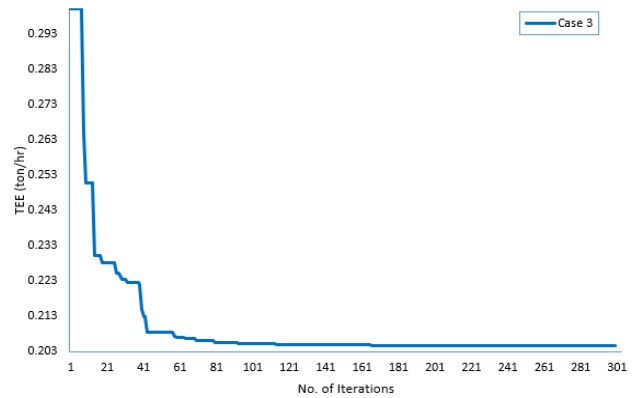
$$a_{ij} = w_j \frac{x_{ij}}{\sqrt{\sum_{i=1}^{100} x_{ij}^2}} \quad (43)$$

$$A = \begin{bmatrix} a_{11} & a_{12} & \cdots\cdots & a_{15} \\ a_{21} & a_{22} & \cdots\cdots & a_{25} \\ \vdots & \vdots & \ddots & \vdots \\ a_{1001} & a_{1002} & \cdots & a_{1005} \end{bmatrix} \quad (44)$$

where, w is the weighting factor of each OF; i is the number of the current alternative and j is the number of the current criteria; A is the normalized decision matrix. If the weighting factors are equal, the coordinates a_j^* of the positive ideal
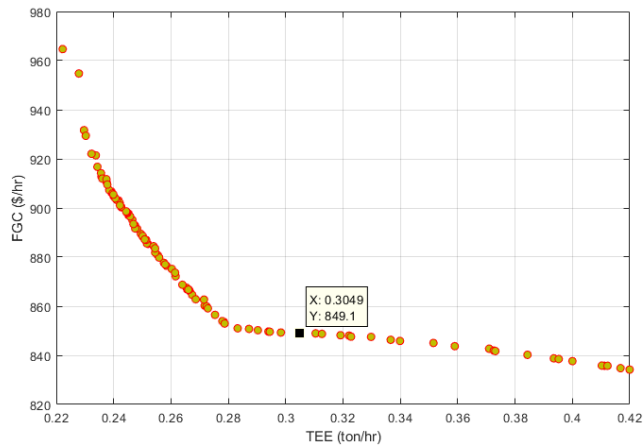
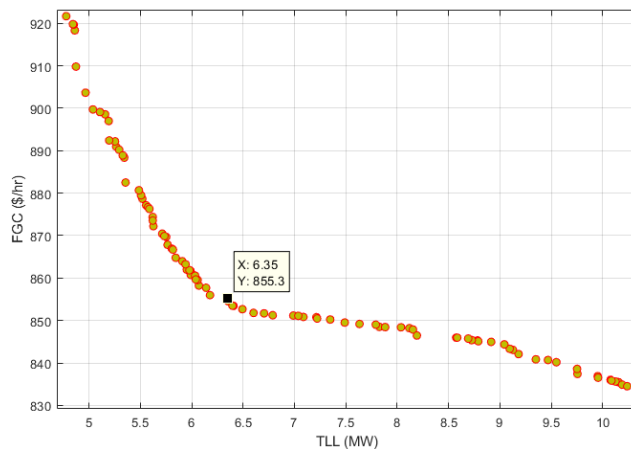**FIGURE 5.** Pareto solutions for Case 4 of the IEEE 30-bus system.

FIGURE 6. Pareto solutions for Case 5 of the IEEE 30-bus system.

solution $A^* = (a_1*, a_2*, \ldots, a_5^*)$ is selected according to the type of the OF (maximization or minimization) using the formula:-

$$a_j^* = \begin{cases} \max a_{ij} \ j = 1, \cdots, 5 \text{ for maximization OF} \\ \min a_{ij} \ j = 1, \cdots, 5 \text{ for minimizaition OF} \end{cases} \quad (45)$$

If some of the alternative A_i is equal to A^* so A_i is the optimal solution. If it is not TOPSIS continues. Selecting the coordinates $a_j^\diamond$ of the negative ideal solution $A^\diamond = (a_1^\diamond, a_2^\diamond, \ldots, a_5^\diamond)$ according to the type of the problem (maximization or minimization) using the formula:-

$$a_j^\diamond = \begin{cases} \min a_{ij} \ j = 1, \cdots \cdots 5 \text{ for maximization OF} \\ \max a_{ij} \ j = 1, \cdots \cdots 5 \text{ for minimizaition OF} \end{cases} \quad (46)$$

Then, the Euclidean distance between each normalized decision vector and the ideal solutions is calculated as follows:

$$d_i^* = d(A_i, A^*) = \sqrt{\sum_{j=1}^{5} (a_{ij} - a_j^*)^2} \quad (47)$$

$$d_i^\diamond = d(A_i, A^\diamond) = \sqrt{\sum_{j=1}^{5} (a_{ij} - a_j^\diamond)^2} \quad (48)$$

where, d_i^* and $d_i^\diamond$ are the deviational values from and the positive and negative ideal solution, respectively.

After that, the relative closeness parameter (D_i) for each Pareto solution (i) is estimated as:

$$D_i = \frac{d_i^\diamond}{d_i^* + d_i^\diamond} \quad (49)$$

V. SIMULATION RESULTS

The proposed IMRFO is applied on two power systems. The first system is the conventional IEEE 30-bus system, as an AC meshed power system, while the second one is
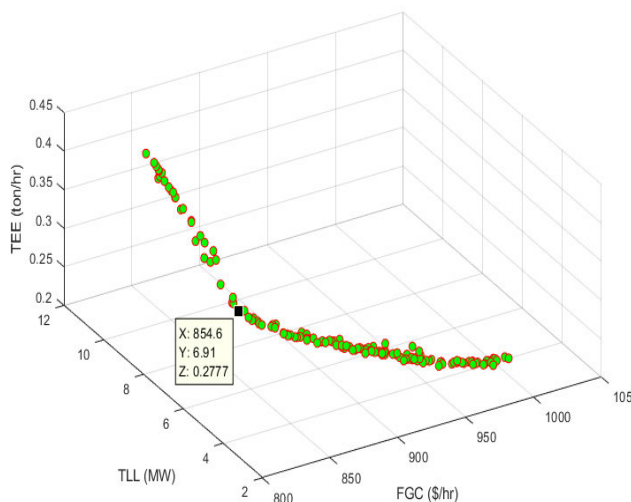
FIGURE 7. Pareto solutions for Case 6 of the IEEE 30-bus system.

the modified IEEE 30-bus with emerged VSC stations, as a hybrid AC/MDC meshed power system.

A. SIMULATION RESULTS OF THE IEEE 30-BUS TEST SYSTEM

This system originally consists of 30 buses, 41 lines, 6 generators, 4 on-load tap changing transformers and 9 shunt capacitive sources as depicted in Fig. 3.

All data of transmission lines, system buses, and the limits of reactive power generations are taken from [40]. The maximum and minimum limits of the load buses voltages and tap changing transformer are 1.1 and 0.9 p.u., respectively. The maximum and minimum values for the generator voltage are 1.1 and 0.95 p.u., respectively. The VAR injections of the capacitive sources are limited by 5 MVA [41]. The proposed IMRFO is applied with number of solutions of 25 and maximum number of iterations of 300.

Six cases are considered for this system including single and multi-objectives as;

TABLE 5. Simulation results for Case 1 of the AC/MDC system.

	Initial	GWO	PSO	SSA	MVO	DA	CSO	BAT	MPO	Proposed Algorithm
Vg 1	1.05	1.053	1.064	1.090	1.100	1.064	1.037	1.069	1.083	1.079
Vg 2	1.04	1.029	1.042	1.077	1.087	1.046	1.026	1.044	1.066	1.061
Vg 5	1.01	0.997	1.006	1.055	1.066	1.042	1.016	1.011	1.047	1.040
Vg 8	1.01	1.008	1.007	1.063	1.065	1.033	1.009	1.022	1.052	1.045
Vg 11	1.05	1.020	1.036	1.003	1.036	1.019	0.994	1.073	0.994	1.007
Vg 13	1.05	0.999	0.983	1.037	1.052	1.062	0.985	1.030	1.000	1.054
T 6-9	1.078	1.044	1.086	1.079	1.053	1.075	1.009	1.070	1.079	1.024
T 6-10	1.069	1.042	0.993	1.021	1.022	1.037	0.974	0.989	1.089	1.071
T 4-12	1.032	1.029	1.039	1.005	1.067	0.951	1.019	1.047	1.053	1.038
T 28-27	1.068	1.040	1.030	1.059	0.989	1.073	1.067	1.010	1.073	1.026
Qc 10	19	8.941	13.000	11.489	8.023	15.385	14.333	4.893	4.255	13.996
Qc 12	0	3.502	13.585	15.504	12.220	18.683	15.647	9.097	5.387	1.765
Qc 15	0	7.311	12.268	15.670	25.200	2.877	14.051	12.982	13.270	6.480
Qc 17	0	5.789	10.000	14.848	14.550	17.780	19.179	2.798	0.687	5.723
Qc 20	0	9.884	7.420	12.362	0.987	3.108	5.550	14.936	5.112	2.670
Qc 21	0	3.288	15.137	12.371	25.880	19.128	16.581	7.270	18.380	12.793
Qc 23	0	14.498	4.615	15.418	2.429	13.719	1.917	7.425	6.672	3.047
Qc 24	4.3	11.900	7.428	17.642	1.043	7.477	3.478	2.983	12.150	6.527
Qc 29	0	9.247	12.139	15.647	5.003	16.793	5.789	7.223	5.706	1.198
Pg 1	105.32	199.79	199.91	156.06	199.99	190.93	199.94	199.36	200.00	200.00
Pg 2	80	37.623	43.234	43.970	34.590	38.828	38.836	31.856	44.010	44.835
Pg 5	50	17.964	18.835	32.824	15.750	24.104	17.995	17.470	17.120	18.601
Pg 8	20	14.424	11.141	18.889	23.600	15.428	12.288	20.819	11.870	10.323
Pg 11	20	13.551	12.591	18.504	11.280	15.314	16.438	10.238	11.550	10.660
Pg 13	20	15.516	12.000	25.301	12.000	13.094	12.173	17.743	12.000	12.007
Qs1	17.31	-4.777	-4.249	7.204	-3.939	-40.509	-27.159	-2.695	-12.220	0.431
Qs4	-17.45	-33.052	-15.975	-26.786	-78.890	-6.292	-63.221	19.342	-34.100	-19.485
Vc2	1	1.011	1.018	1.067	1.072	1.029	1.016	1.029	1.056	1.051
Vc3	1	1.020	0.961	0.940	1.039	1.055	0.980	1.018	0.998	0.999
Vc5	1	0.989	0.995	1.053	1.063	1.028	1.008	1.025	1.006	1.041
Vc6	1	0.966	0.979	1.071	1.043	0.979	1.018	1.018	1.009	1.041
Ps2	25.74	3.563	3.350	6.033	-1.013	26.856	20.249	23.239	13.000	14.067
Ps3	52.53	6.129	18.906	13.731	7.800	24.427	26.984	13.838	32.430	31.285
Ps5	40.44	13.717	31.442	14.478	42.540	37.488	24.000	23.903	41.640	36.818
Ps6	18.45	7.708	23.908	23.555	11.800	10.763	18.797	21.931	18.210	18.374
Vdc,1	1.06	1.011	1.012	0.971	0.912	1.035	1.035	0.970	1.100	1.083
Vdc,4	1.06	1.062	1.012	1.083	1.098	1.025	0.967	0.912	1.100	1.072
FGC ($/hr)	**975.64**	**854.43**	**846.25**	**885.46**	**849.17**	**858.47**	**848.93**	**853.13**	**841.45**	**840.3**
TEE (ton/hr)	0.242	0.436	0.439	0.306	0.438	0.403	0.437	0.435	0.440	0.440
TLL (MW)	11.924	15.475	14.309	12.150	13.819	14.301	14.274	14.089	13.155	13.026

Case 1: Minimization of the FGC;

Case 2: Minimization of the TLL;

Case 3: Minimization of the TEE;

Case 4: Minimization of the FGC and TEE bi-objective functions;

Case 5: Minimization of the FGC, the TLL bi-objective functions;

Case 6: Minimization of the sinusoidal model of FGC, the TEE and the TLL tri-objective functions.

1) RESULTS OF SINGLE OBJECTIVE OPF

Tables 2 tabulates the optimal values of the decision variables and the related results of the algorithm for a single objective of FGC, TLL and TEE minimization for Cases 1-3 respectively.

Firstly, the FGC objective model of Eq. (4) is considered which as Case 1A and the proposed IMRFO is applied. From Table 2, the FGC objective is reduced from 975.64 to 830.6795 $/h with a reduction of 14.86%

compared with the initial case. Secondly, the quadratic model of the FGC objective is considered in Case 1B neglecting the valve loading point. In this case, the proposed algorithm can minimize the FGC to 798.99 $/h. Table 3 provides comparisons for minimizing the FGC (Case 1A) for the IEEE 30-bus system considering several reported algorithms in the literature. As shown, the proposed algorithm has great outperformance compared with artificial bee colony (ABC) [42], teaching-learning algorithm [43], differential evolution (DE) [41], symbiotic organisms search (SOS) [44], moth swarm algorithm (MSA) [45], developed grey wolf algorithm (DGWA) [46], improved moth flame algorithm (IMFA) [47], grasshopper optimizer (GO) [48], adaptive grasshopper optimizer (AGO) [48].

In the second case, the TLL objective is reduced from 5.596 to 2.846 MW with a reduction of 49.14% compared with the initial case. In the third case, the TEE objective is reduced from 0.2390963 to 0.204754 ton/h. Table 4 provides comparisons for minimizing the TEE (Case 3) for the

TABLE 6. Simulation results for Case 2 of the AC/MDC system.

	GWO	PSO	SSA	MVO	DA	CSO	BAT	MPO	Proposed Algorithm
Vg 1	1.052	1.024	1.076	1.096	1.074	1.028	1.076	1.066	1.0895
Vg 2	1.039	1.015	1.061	1.09	1.068	1.018	1.068	1.064	1.0863
Vg 5	1.021	0.9977	1.034	1.076	1.06	1.001	1.047	1.051	1.0743
Vg 8	1.023	0.997	1.047	1.08	1.052	0.9939	1.057	1.058	1.0808
Vg 11	1.03	0.9834	0.9957	0.9832	1.058	1.06	1.064	0.9764	1.0286
Vg 13	0.9915	0.9961	1.032	1.024	1.07	1.032	1.053	1.035	1.0527
T 6-9	0.9958	1.07	1.062	1.095	1.028	1.005	1.095	1.061	1.0791
T 6-10	1.068	0.95	1.057	0.9913	1.062	1.056	1.038	1.082	1.0257
T 4-12	1.015	0.9687	0.9919	1.08	0.9773	0.9508	1.071	1.043	1.0473
T 28-27	1.032	0.9692	1.028	1.062	1.045	1.015	1.071	1.037	1.0405
Qc 10	6.453	20.28	19.25	4.341	5.84	14.83	12.02	9.064	10.843
Qc 12	4.491	8.495	11.51	24.39	16.35	15.62	20.83	0.00223	16.409
Qc 15	10.15	18.92	20.17	4.806	10.4	11.68	2.781	11.31	4.5768
Qc 17	11	8.423	16.03	14.36	11.09	10.3	11.52	7.855	7.3967
Qc 20	5.157	3.758	12.25	5.509	7.028	8.373	15.5	0.2161	6.3678
Qc 21	4.086	6.467	8.911	12.87	7.322	12.64	0.2179	29.61	7.7028
Qc 23	7.542	4.51	15.59	1.779	17.04	10.61	5.122	4.559	1.717
Qc 24	6.322	3.892	11.85	8.106	9.34	5.553	7.141	0.1119	7.6287
Qc 29	1.669	2.105	17.14	3.024	15.11	6.103	2.389	3.128	5.6515
Pg 1	115.298	72.788	145.931	93.845	89.2841	83.407	77.744	57.6204	59.319
Pg 2	68.55	73.29	52.35	66.21	71.38	79.21	70.26	80	79.524
Pg 5	42.14	49	27.22	50	48.42	49.8	49.72	50	49.976
Pg 8	29.24	31.4	21.94	32.95	32.71	26.42	30.62	35	34.807
Pg 11	17.16	30	20.53	28.64	25.01	23.15	24.81	30	29.996
Pg 13	21.86	36	28.23	20.76	26.4	30.99	39.69	39.53	38.348
Qs1	-7.134	11.65	-11.12	18.46	0.7159	-8.617	-11.8	13.3	10.975
Qs4	-11.62	10.04	17.1	-24.08	2.023	-2.627	-6.299	-22.94	16.769
Vc2	1.023	0.9998	1.051	1.082	1.06	1.004	1.063	1.06	1.0839
Vc3	1.006	1.054	0.9459	1.013	1.057	0.9637	1.036	0.9317	0.99268
Vc5	0.9865	1.015	1.042	1.027	1.065	1.044	1.03	1.018	1.0461
Vc6	0.9893	1.03	1.05	1.024	1.033	1.003	0.9965	1.013	1.0457
Ps2	0.1408	11.1	21.94	8.673	6.849	7.77	6.444	10.7	3.7913
Ps3	29.29	24.02	-1.462	16.56	26.07	25.09	8.285	18.13	19.044
Ps5	-0.6621	15.22	5.95	13.8	12.55	18.23	5.617	17.47	16.485
Ps6	12.89	13.83	14.23	13.57	14.11	9.988	15.29	10.02	13.756
Vdc,1	1.051	1.049	1.042	1.088	1.022	1.033	1.088	1.1	1.1
Vdc,4	0.9892	0.9889	1.035	1.099	1.032	0.9316	1.02	1.1	1.0954
FGC ($/hr)	932.3	1022.2	885.7	986.9	991.8	1005.2	1021.0	1043.7	1039.8
TEE (ton/hr)	0.246	0.208	0.286	0.222	0.219	0.219	0.210	0.205	0.205
PLAC	3.443	1.522	5.490	1.767	2.266	1.991	2.406	1.451	1.328
PLVSC	6.886	6.957	6.936	6.897	6.952	6.968	6.847	6.917	6.862
PLDC	0.519	0.598	0.375	0.342	0.586	0.618	0.192	0.382	0.380
TL (MW)	**10.848**	**9.078**	**12.801**	**9.005**	**9.804**	**9.577**	**9.445**	**8.750**	**8.570**

IEEE 30-bus system considering several reported algorithms in the literature. As shown, the proposed algorithm has great outperformance compared to artificial bee colony (ABC) [42], krill herd algorithm (KHA) [49], stud krill herd algorithm (SKHA) [49], adaptive real coded biogeography-based optimization (ARBO) [50], teaching learning-based optimization (MTLBO) [51], modified teaching learning-based optimization (MTLBO) [51], grasshopper optimizer (GO) [48], adaptive grasshopper optimizer (AGO) [48].

Figs. 4 a, b, and c display the convergence characteristics of the proposed algorithm for the Cases 1-3 that describe the high capability of the proposed IMRFO in finding the minimum considered objective. The progress through the iterations illustrates the ability to evolutionarily search for the optimal solution.

2) RESULTS OF MULTI-OBJECTIVE OPF OPTIMIZATION

In this subsection, a multi objective optimization of OPF is performed using the proposed IMRFO for bi-objective (Cases 4 and 5) and tri-objective functions (Case 6). Table 2 shows the values of the decision variables and the corresponding results for Cases 4-6. Figs. 5-7 display, respectively, the Pareto set solutions for OPF with bi-objective functions FGC and TEE minimization (Case 4), bi-objective functions FGC and TLL minimization (Case 5) and tri-objective functions FGC, TEE and TLL minimization (Case 6). The obtained result in these figures clarify that the capability of the proposed IMRFO to extract best compromise of the objective functions. In comparison with Cases 1-3, the best compromise FGC, TEE and TLL are close to the single objective achieved values. Fig. 8 shows the voltage profile of

TABLE 7. Simulation results for Case 3 of the AC/MDC system.

	GWO	PSO	SSA	MVO	DA	CSO	BAT	MPO	Proposed Algorithm
Vg 1	1.034	1.061	1.095	0.9792	1.069	0.9884	1.017	1.066	0.99938
Vg 2	1.032	1.044	1.082	0.9767	1.073	1.008	1.016	1.06	0.99684
Vg 5	0.9962	1.031	1.055	0.95	1.047	1.008	1.04	1.05	0.98779
Vg 8	1.032	0.9998	1.064	0.9651	1.056	1.001	1.042	1.051	0.99063
Vg 11	1.062	1.053	1.002	1.063	1.012	1.06	1.057	1.062	0.98074
Vg 13	1.051	0.9741	1.046	1.012	1.068	1.011	1.085	1.065	1.0378
T 6-9	0.947	0.9754	1.09	0.9627	1.064	1.065	1.03	1.097	0.97347
T 6-10	0.9648	1.015	1.015	1.099	1.054	1.032	1.053	1.095	1.0588
T 4-12	1.077	1.021	1.033	1.035	1.031	0.949	0.9795	1.012	1.0048
T 28-27	1.006	1.068	1.054	1.012	1.028	1.016	1.076	1.043	1.0048
Qc 10	14.26	13.6	16.29	26.81	6.106	7.486	23.1	27.53	7.9286
Qc 12	4.704	6.773	15.41	1.993	24.95	1.712	28.12	23.59	6.5109
Qc 15	10.38	11.38	14.88	14.38	7.612	18.73	17.16	29.05	4.7955
Qc 17	6.473	14.35	14.51	15.64	14.26	10.12	23.75	15.89	8.3749
Qc 20	6.216	15.89	14.88	7.079	7.173	21.07	3.252	8.295	4.8516
Qc 21	6.64	12.78	14.73	4.637	8.806	18.09	2.578	15.74	17.314
Qc 23	8.098	8.516	13.55	11.18	15.12	7.534	5.132	1.082	0.69503
Qc 24	20.66	8.889	13.05	4.092	2.681	4.803	2.962	18.86	15.257
Qc 29	8.036	7.423	16.39	12.15	16.29	8.495	25.61	15.9	6.4305
Pg 1	76.54	65.23	136.8	66.07	99.09	76.73	85.2055	67.56	67.003
Pg 2	68.86	76	60.32	72.43	66.11	65.75	65.56	70.46	70.452
Pg 5	49.95	50	30.77	50	50	49.72	49.16	50	49.989
Pg 8	34.36	34	23.36	35	24.08	34.51	35	35	34.988
Pg 11	29.59	30	20.77	30	23.43	29.9	28.71	30	29.996
Pg 13	37.94	40	24.53	40	31.83	39.07	37.44	40	39.994
Qs1	-69.19	-44.98	-3.733	6.621	33.71	13.72	-35.97	0.6827	-0.67811
Qs4	-22.57	59.46	-32.37	-24.11	-38.07	-80.87	-11.84	-28.71	-27.32
Vc2	1.029	0.9982	1.069	0.9676	1.064	1.001	1.038	1.058	0.9925
Vc3	1.003	0.9536	0.9607	0.9124	0.9979	0.9393	1.033	1.099	1.0469
Vc5	1.046	0.9864	1.043	0.99	1.051	0.9736	1.071	1.066	1.0107
Vc6	0.9514	0.9735	1.075	0.9379	1.064	0.9081	1.016	1.059	0.99316
Ps2	-0.8581	-25.44	-0.2309	1.102	17.48	-3.586	2.877	1.751	7.3397
Ps3	-36.5	36.31	2.616	5.303	42.19	43.22	-53.27	23.4	10.905
Ps5	11.61	14.35	-7.893	3.932	-0.9449	0.3515	-12.96	1.699	15.449
Ps6	4.079	19.24	27.98	9.282	16.51	-3	16.09	12.71	12.235
Vdc,1	0.9466	0.9709	0.9033	1.046	1.052	0.9774	0.9339	1.099	1.0321
Vdc,4	0.9818	1.07	1.048	1.07	1.002	1.068	0.9699	1.099	1.092
FGC ($/hr)	1042.5	1048.9	889.9	1041.1	992.2	1037.1	1044.4	1037.7	1035.7
TEE (ton/hr)	**0.207**	**0.205**	**0.273**	**0.204**	**0.225**	**0.206**	**0.211**	**0.2033**	**0.2031**
TLL (MW)	13.842	11.820	13.204	10.102	11.142	12.293	17.675	9.623	9.022

the AC power system for the initial case, single objective OPF cases, and multi-objective cases using the proposed IMRFO. As shown, all the buses voltages are within the allowable limits. In addition, high improvement is illustrated since the minimum voltage at the initial case of 0.9012 pu. at bus 30 becomes 1.0712 pu. for Case 1A, 1. 07056 pu. for Case 1B, 1. 06912 pu. for Case 2, 1.02923 pu. for Case 3, 1.0501 pu. for Case 4, 1.0303 pu. for Case 5, and 1.0272 pu. for Case 6.

B. SIMULATION RESULTS OF THE MODIFIED IEEE 30-BUS WITH EMERGED VSC STATIONS

The IEEE 30-bus is modified with emerged VSC stations, as a hybrid ac/mdc meshed power system. The modified system has two MDC grids [28] as depicted in Fig. 9. The control mode of the VSCs in the first MDC grid of the modified 30-bus system are; VSC 1 is V_{dc}-Q_c control mode, VSCs 2 and 3 are in P_{dc}-V_c constant control. In the second MDC grid, VSC 4 is V_{dc}-Q_c control mode whilst VSCs 5 and 6 are in P_{dc}-V_c constant control. The

converting power for the VSCs are considered of 100 MVA where the maximum and minimum voltages of the VSCs and DC buses are 1.1 and 0.9 p.u., respectively. The VAR injections of the capacitive sources are limited by 5 MVA. To evaluate the effectiveness of the proposed IMRFO, various recent algorithms are employed for the same target such as GWO [52]; PSO; SSA [38]; MVO [53]; dragonfly algorithm (DA) [54]; crow search optimization algorithm (CSO) [55], [56]; Bat algorithm (BAT) [57], [58]; Marine predator optimizer (MPO) [59] are employed to solve the considered problem. The competitive algorithms have the same number of solutions (50) while the IMRFO has half these number of solutions as it provides two function evaluation in the iteration. They are 15 independent runs are considered.

1) RESULTS OF SINGLE OBJECTIVE OPF

In this subsection, the proposed IMRFO and several competitive techniques are applied for optimal operation of hybrid AC/MDC system with a single objective of FGC, TLL and
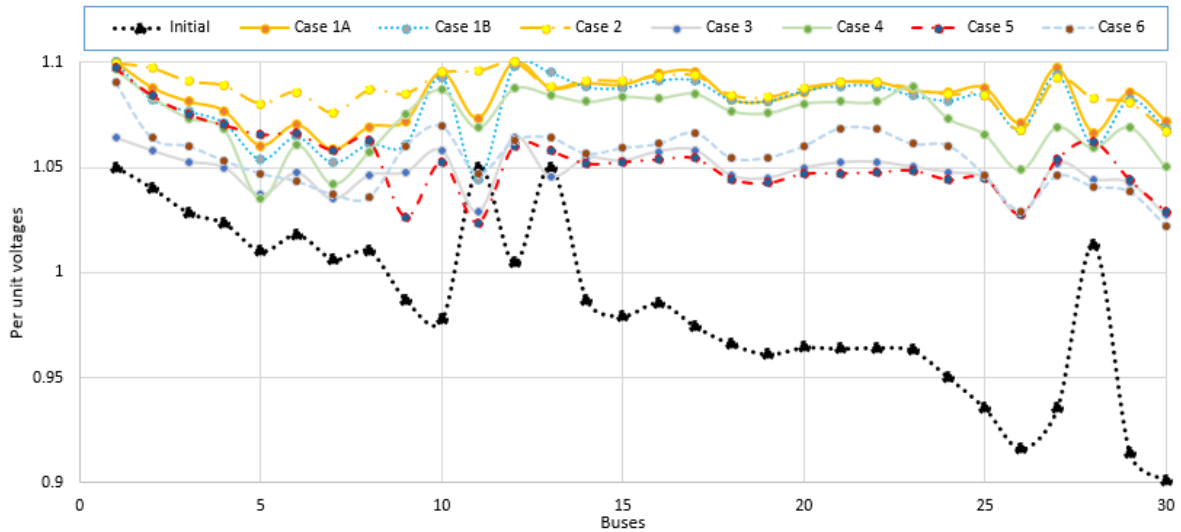
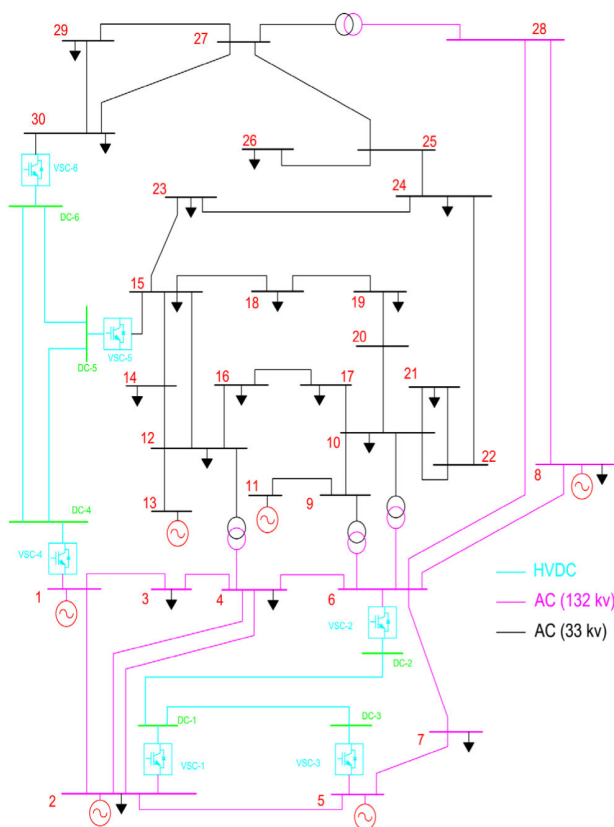**FIGURE 8.** Voltages of the AC grid of the IEEE 30-bus system.

FIGURE 9. Modified IEEE 30-bus system with six emerged VSC stations and two MDC power systems.

FIGURE 10. Convergence rates of IMRFO Case 1.

TEE minimization for Cases 1-3, respectively. The optimal values of the decision variables and the regarded results are given in Tables 5-7, respectively. As shown, from the obtained results the FGC, given in Table 5, is reduced from 975.64 to 840.3 $/h with a reduction of 13.87% compared

with the initial case using the IMRFO, while the reduction percentage using the GWO, PSO, SSA, MVO, DA, CSO, BAT and MPO are 12.42%, 13.26%, 9.24%, 12.96%, 12.01%, 12.99%, 12.56% and 13.75%, respectively, compared with the initial case. Fig. 10 displays the convergence rates of the compared algorithms for handling Case 1. It declares the great characteristics of the proposed IMRFO in developing the best solution compared to the others.

Also, the proposed technique succeeds in achieving the minimum TLL which is the primary objective function in Case 2. It is superior to other techniques as listed in Table 6. The total power losses are reduced from 11.924 MW to 8.57 MW with a reduction of 28.12% using the proposed MRFO while the reduction achieved by other competitive techniques are 9.02%, 23.87%, -7.36%, 24.48%, 17.78%, 19.68%, 20.79% and 26.62% using the GWO, PSO, SSA, MVO, DA, CSO, BAT and MPO, respectively. For handling Case 2, Fig. 11 displays the convergence rates of the
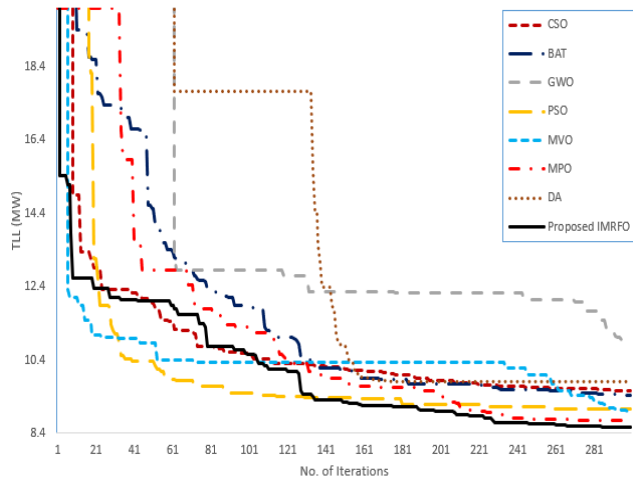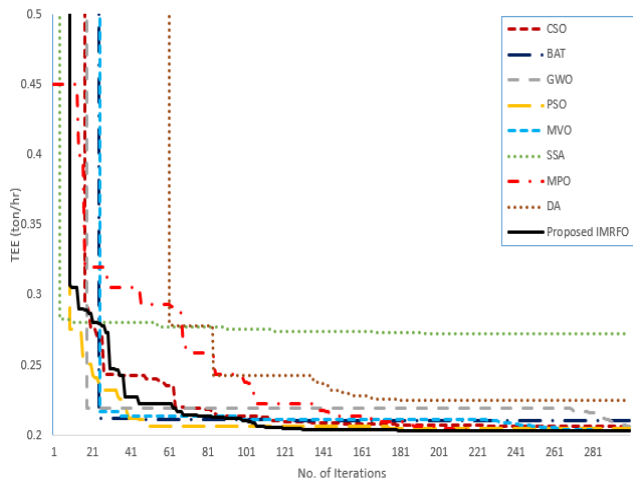
FIGURE 11. Convergence rates of IMRFO Case 2.

FIGURE 12. TEE minimization convergence rates of IMRFO for Case 3.

TABLE 8. Multi-objective simulation results for IEEE 30-bus system.

	Initial	Case 4	Case 5	Case 6
Vg_1	1.05	1.0631	1.0597	1.0955
Vg_2	1.04	1.0496	1.0447	1.0729
Vg_5	1.01	1.0078	1.0198	1.0517
Vg_8	1.01	1.0177	1.024	1.062
Vg_{11}	1.05	1.0530	0.9876	1.0529
Vg_{13}	1.05	1.0248	1.0242	1.081
T_{6-9}	1.078	1.0116	1.0626	1.0585
T_{6-10}	1.069	0.9907	1.0703	1.0314
T_{4-12}	1.032	1.0517	1.05	1.0126
T_{28-27}	1.068	1.0591	1.0324	1.0198
Qc_{10}	19	9.1078	14.0935	6.7464
Qc_{12}	0	18.5561	8.5547	19.0608
Qc_{15}	0	22.5916	16.2232	15.0916
Qc_{17}	0	3.4197	19.4305	20.0593
Qc_{20}	0	10.4293	11.7345	5.2101
Qc_{21}	0	8.0745	12.0721	5.3426
Qc_{23}	0	4.3556	5.2854	4.3013
Qc_{24}	4.3	14.3683	9.1136	5.316
Qc_{29}	0	5.0922	10.0738	8.8216
Pg_1	105.323	147.3954	158.3223	129.3655
Pg_2	80	62.0709	41.7601	66.2022
Pg_5	50	21.5073	20.2803	22.6008
Pg_8	20	28.6463	32.5656	32.8303
Pg_{11}	20	16.3659	25.3886	22.9121
Pg_{13}	20	19.5660	16.8085	20.3413
Qs_1	17.31	-38.7768	-30.1316	-43.7106
Qs_4	-17.45	-44.5952	-13.6828	3.0458
Vc_2	1	1.0209	1.0291	1.0688
Vc_3	1	1.0327	1.0243	1.0457
Vc_5	1	1.0166	1.0303	1.0785
Vc_6	1	1.0522	1.0322	1.0821
Ps_2	25.74	10.8735	1.2916	16.1855
Ps_3	52.53	17.3946	34.173	21.0756
Ps_5	40.44	29.4673	36.3295	26.2714
Ps_6	18.45	18.0010	15.9309	12.7149
$V_{dc,1}$	1.06	1.0150	1.0395	1.078
$V_{dc,4}$	1.06	1.0256	1.0833	1.0156
FGC ($/hr)	975.64	**870.9**	873.7721	882.5743
TEE (ton/hr)	0.2417	**0.294988**	0.3119625	**0.264915**
TLL (MW)	11.9237	12.15184	**11.72543**	10.85332

compared algorithms which states the great characteristics of the proposed IMRFO in developing the best solution compared to the others.

Similarly, the proposed technique succeeds in achieving the minimum TEE, Case 3, which is reduced from 0.242 to 0.203 ton/hr by a reduction of 16.11%, while other techniques
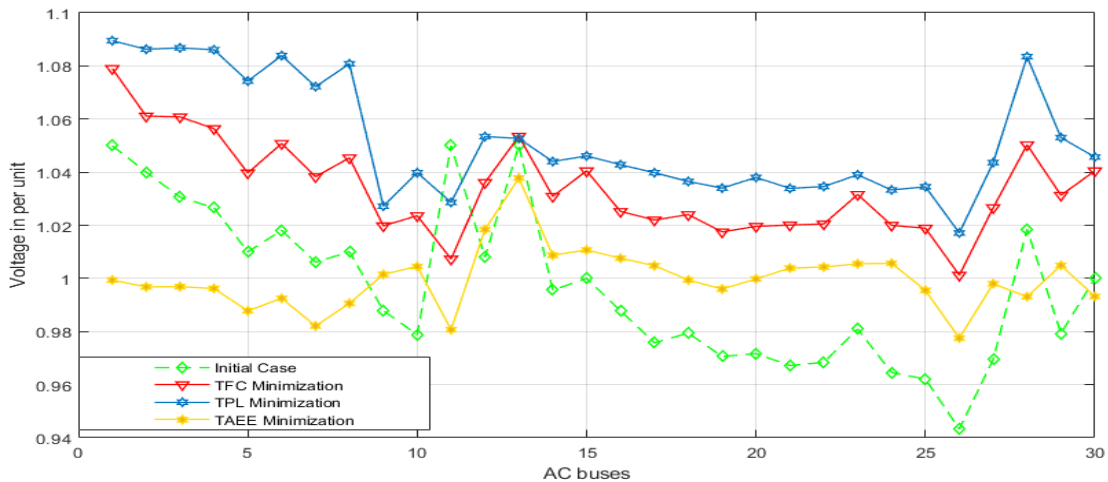

FIGURE 13. Voltages of the AC grid for Cases 1-3.

can't achieve this value as given in Table 7. In this table, another achievement is noticed in the technical point of view with power losses reduction by 24.3 %. Fig. 12 shows the convergence rates of the proposed algorithm compared to the other recent algorithms for Case 3. From this figure, the high capability of the IMRFO in finding the minimum considered objective is clarified compared to the others. The progress through the iterations illustrates the ability to evolutionarily search for the optimal solution.

These results illustrate that the proposed algorithm outperforms the others to optimally operate the hybrid AC/MDC power system for single objective cases with significant achievement for each separate objective function.

Also, the voltage profile of the Ac grids is greatly improved with the proposed technique as shown in Fig. 13.

2) RESULTS OF MULTI-OBJECTIVES OPF FOR THE AC/MDC SYSTEM

The complexity of OPF of the hybrid AC/MDC systems as well as the variety of the decision variables makes it difficult for most of the competitive techniques to achieve the optimal solution especially for multi-objective cases. therfore, a multi objective OPF optimization in hybrid AC/MDC systems are hamdled via the proposed IMRFO for bi-objective and tri-objective functions.

Table 8 shows the decision variables' settings and the corresponding results for the three multi-objective cases. Figs. 14-16 depict, respectively, the Pareto set solutions for optimal operation of AC/MDC with bi-objective functions FGC and TEE minimization (Case 4), bi-objective functions FGC and TLL minimization (Case 5) and tri-objective functions FGC, TEE and TLL minimization (Case 6). The obtained results in these figures clarify that the proposed IMRFO gives best compromise of the objective functions. In comparison with Cases 1-3, the best compromise FGC, TEE and TLL are close to the single objective achieved
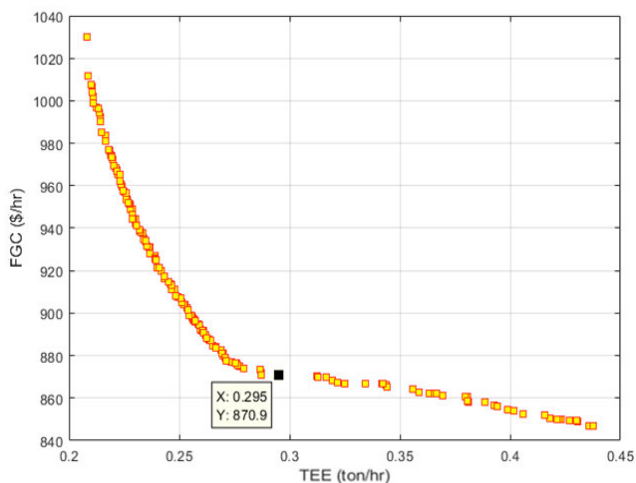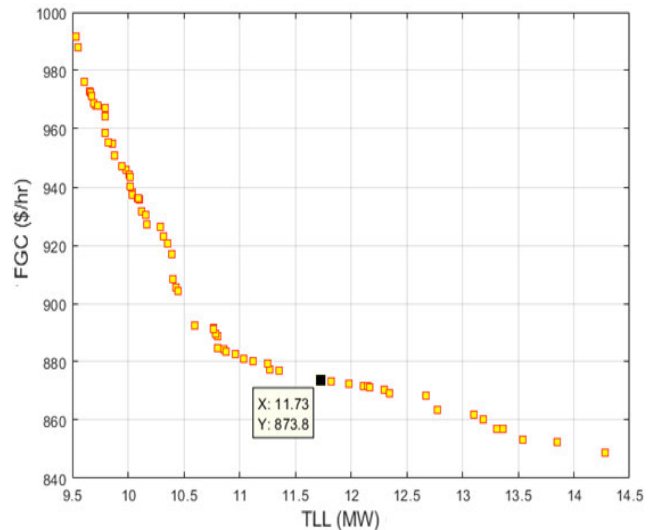

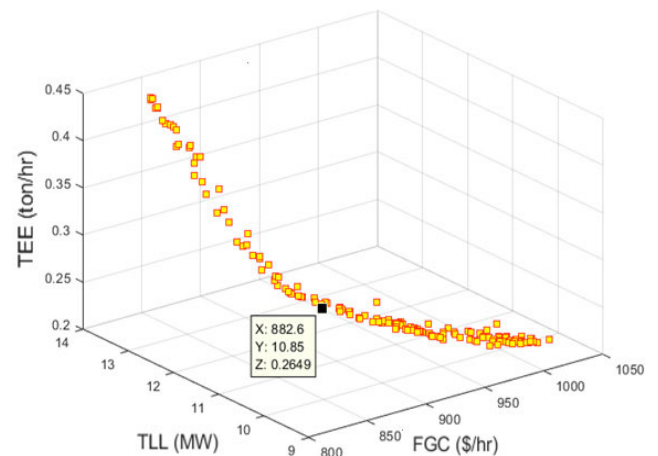**FIGURE 15.** Pareto solutions for Case 5.

FIGURE 16. Pareto solutions for Case 6.

values. In Case 4, the available compromise solutions, between FGC minimization and TEE minimization, are obtained starting from FGC about 840 ($/hr) and TEE about 0.44 (ton/hr) to FGC about 10432 ($/hr) and TEE about 0.209 (ton/hr) passing through the optimal solution FGC of 870.9 ($/hr) and TEE of 0.295 (ton/hr) as shown in Fig. 14.

In Case 5, several compromise solutions are obtained between FGC minimization and TLL minimization starting from FGC about 848 ($/hr) and TLL about 14.3 (MW) to FGC about 994 ($/hr) and TLL about 9.5 (MW) passing through the optimal solution FGC of 873.8 ($/hr) and TLL of 11.73 (MW) as shown in Fig. 15. Similarly, in Fig. 16 well-distributed solutions are obtained including the optimal compromise solution of FGC of 882.6 ($/hr), TEE of 0.2649 (ton/hr) and TLL of 10.85 (MW). Fig. 17 shows the voltage profile of AC grid for the initial case, and multi-objective cases using the proposed IMRFO, where all buses voltages are within the allowable limits.
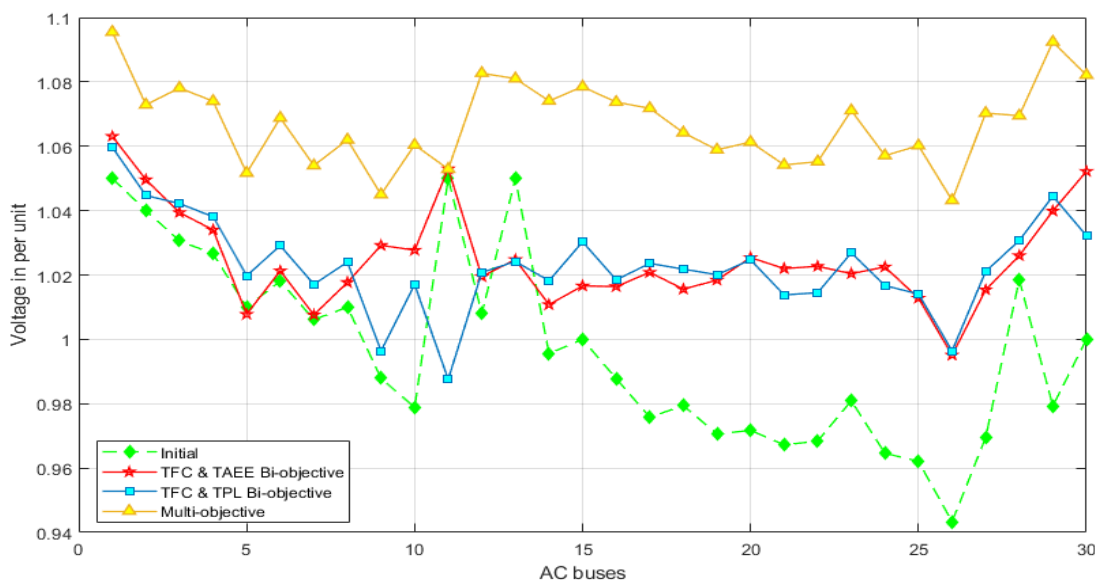

FIGURE 14. Pareto solutions for Case 4.

FIGURE 17. Voltages of AC grid for multi-objective cases.

VI. CONCLUSION

In this paper, an improved version of manta ray foraging algorithm (IMRFO) has been presented for the optimal operation of AC meshed and hybrid AC/MDC meshed power systems with emerged VSC stations. The multi-objective formulation of optimal operation of the hybrid grid aims at minimizing the total fuel costs, the total atmospheric environmental emissions related to the generation stations and minimizing the total power losses in the VSCs stations, AC, and MDC power systems. The proposed IMRFO mimics three distinct individual foraging organizations of the manta rays. It is upgraded integrating an external Pareto repository to conserve the non-dominated manta ray's positions. Furthermore, a TOPSIS is utilized to select the final candidate operating point of the hybrid AC/MDC power grid. The applicability of the proposed IMRFO has been verified through conventional IEEE 30-bus system, as an AC meshed power system, and modified IEEE 30-bus with emerged VSC stations, as a hybrid AC/MDC meshed power system. Assessment of the proposed solution methodology is employed with significant improvements compared with several recent algorithms. Significant technical improvements are achieved with reducing the power losses as well as the environmental emissions. The simulation results demonstrate the effectiveness and preponderance of the proposed algorithm with great stability indices over the others for single and multi-objective cases. Nevertheless, the proposed method has well-diversified Pareto solutions while a compromise operating point is effectively produced to satisfy the operator requirements.

REFERENCES

[1] A. Eltved, J. Dahl, and M. S. Andersen, "On the robustness and scalability of semidefinite relaxation for optimal power flow problems," *Optim. Eng.*, vol. 21, no. 2, pp. 375–392, Jun. 2020.

[2] E. Mohagheghi, M. Alramlawi, A. Gabash, and P. Li, "A survey of real-time optimal power flow," *Energies*, vol. 11, no. 11, p. 3142, Nov. 2018, doi: 10.3390/en11113142.

[3] F. Zohrizadeh, C. Josz, M. Jin, R. Madani, J. Lavaei, and S. Sojoudi, "A survey on conic relaxations of optimal power flow problem," *Eur. J. Oper. Res.*, vol. 287, no. 2, pp. 391–409, Dec. 2020.

[4] M. Aragüés-Peñalba, T. L. Nguyenb, R. Caireb, A. Sumpera, S. Galceran-Arellano, and Q.-T. Tranb, "General form of consensus optimization for distributed OPF in HVAC-VSCHVDC systems," *Electr. Power Energy Syst.*, vol. 121, Oct. 2020, Art. no. 106049.

[5] M. Hotz and W. Utschick, "Hynet: An optimal power flow framework for hybrid AC/DC power systems," *IEEE Trans. Power Syst.*, vol. 35, no. 2, pp. 1036–1047, Mar. 2020.

[6] A. Korompili, Q. Wu, and H. Zhao, "Review of VSC HVDC connection for offshore wind power integration," *Renew. Sustain. Energy Rev.*, vol. 59, pp. 1405–1414, Jun. 2016.

[7] ABB. *Zhangbei: The World's First DC-Grid with HVDC Light.* [Online]. Available: https://new.abb.com/systems/hvdc/references/zhangbei

[8] M. Gul, N. Tai, W. Huang, M. H. Nadeem, M. Ahmad, and M. Yu, "Technical and economic assessment of VSC-HVDC transmission model: A case study of south-western region in Pakistan," *Electronics*, vol. 8, no. 11, p. 1305, Nov. 2019.

[9] *Fifth Power System Development Project: Environmental Assessment (Vol. 18) : 800 kV, 3000 MW HVDC Bipole Between Champa Pooling Station and Kurukshetra (WR-NR Interconnector for IPP Projects in Chattishgarh).* [Online]. Available: https://documents.worldbank.org/curated/en/397261468267582972/pdf/E20890v180EA0I00Box385346B00PUBLIC0.pdf

[10] R. A. Valiquette, "HVDC life extension for Nelson river HVDC system," in *Proc. IEEE Winter Meeting Power Eng. Soc.*, New York, NY, USA, Jan. 2002, pp. 27–31.

[11] *Egyptian Electricity Holding Company Annual Reports 2017–2018.* Accessed: Jan. 2020. [Online]. Available: http://www.moee.gov.eg/english_new/EEHC_Rep/2018-2019en.pdf

[12] European Wind Energy Association, "The European offshore wind industry key 2011 trends and statistics," EWEA, Brussels, Belgium, Tech. Rep. 1, Jan. 2012. [Online]. Available: http://large.stanford.edu/courses/2012/ph240/pratt1/docs/EWEA_stats_offshore_2011_01.pdf

[13] J. F. Chozas, H. C. Soerensen, and M. Korpas, "Integration of wave and offshore wind energy in a European offshore grid," in *Proc. 20th Int. Offshore Polar Eng. Conf.*, vol. 7, Beijing, China, 2010, pp. 926–933.

[14] S. Rodrigues, R. T. Pinto, P. Bauer, and J. Pierik, "Optimal power flow control of VSC-based multiterminal DC network for offshore wind integration in the north sea," *IEEE J. Emerg. Sel. Topics Power Electron.*, vol. 1, no. 4, pp. 260–268, Dec. 2013.

[15] J. Lin, V. O. K. Li, K.-C. Leung, and A. Y. S. Lam, "Optimal power flow with power flow routers," *IEEE Trans. Power Syst.*, vol. 32, no. 1, pp. 531–543, Jan. 2017, doi: 10.1109/TPWRS.2016.2542678.

[16] A. A. Hamad and E. F. El-Saadany, "Multi-agent supervisory control for optimal economic dispatch in DC microgrids," *Sustain. Cities Soc.*, vol. 27, pp. 129–136, Nov. 2016, doi: 10.1016/j.scs.2016.02.016.

[17] V. Donde, X. Feng, I. Segerqvist, and M. Callavik, "Distributed state estimation of hybrid AC/HVDC grids by network decomposition," *IEEE Trans. Smart Grid*, vol. 7, no. 2, pp. 974–981, Mar. 2016.

[18] J. Li, F. Liu, Z. Wang, S. H. Low, and S. Mei, "Optimal power flow in stand-alone DC microgrids," *IEEE Trans. Power Syst.*, vol. 33, no. 5, pp. 5496–5506, Sep. 2018.

[19] S. Sayah, "Modified differential evolution approach for practical optimal reactive power dispatch of hybrid AC-DC power systems," *Appl. Soft Comput.*, vol. 73, pp. 591–606, 2018.

[20] L. Roald and G. Andersson, "Chance-constrained AC optimal power flow: Reformulations and efficient algorithms," *IEEE Trans. Power Syst.*, vol. 33, no. 3, pp. 2906–2918, May 2018.

[21] M. B. Shafik, H. Chen, G. I. Rashed, and R. A. El-Sehiemy, "Adaptive multi objective parallel seeker optimization algorithm for incorporating TCSC devices into optimal power flow framework," *IEEE Access*, vol. 7, pp. 36934–36947, 2019.

[22] J. Duan, W. Zeng, and M.-Y. Chow, "Resilient distributed DC optimal power flow against data integrity attack," *IEEE Trans. Smart Grid*, vol. 9, no. 4, pp. 3543–3552, Jul. 2018.

[23] L. Mackay, R. Guarnotta, A. Dimou, G. Morales-Espana, L. Ramirez-Elizondo, and P. Bauer, "Optimal power flow for unbalanced bipolar DC distribution grids," *IEEE Access*, vol. 6, pp. 5199–5207, 2018.

[24] W. Feng, A. Le Tuan, L. B. Tjernberg, A. Mannikoff, and A. Bergman, "A new approach for benefit evaluation of multiterminal VSC–HVDC using a proposed mixed AC/DC optimal power flow," *IEEE Trans. Power Del.*, vol. 29, no. 1, pp. 432–443, Feb. 2014.

[25] M. Hosseinzadeh and F. R. Salmasi, "Robust optimal power management system for a hybrid AC/DC micro-grid," *IEEE Trans. Sustain. Energy*, vol. 6, no. 3, pp. 675–687, Jul. 2015.

[26] Q. Zhao, J. García-González, O. Gomis-Bellmunt, E. Prieto-Araujo, and F. M. Echavarren, "Impact of converter losses on the optimal power flow solution of hybrid networks based on VSC-MTDC," *Electr. Power Syst. Res.*, vol. 151, pp. 395–403, Oct. 2017.

[27] A. Maulik and D. Das, "Optimal power dispatch considering load and renewable generation uncertainties in an AC–DC hybrid microgrid," *IET Gener., Transmiss. Distrib.*, vol. 13, no. 7, pp. 1164–1176, Apr. 2019.

[28] J. Renedoa, A. Ibrahim, B. Kazemtabrizi, A. García-Cerrada, L. Rouco, Q. Zhao, and J. García-González, "A simplified algorithm to solve optimal power ows in hybrid VSC-based AC/DC systems," *Electr. Power Energy Syst.*, vol. 110, pp. 781–794, Sep. 2019.

[29] A. Lotfjou, Y. Fu, and M. Shahidehpour, "Hybrid AC/DC transmission expansion planning," *IEEE Trans. Power Del.*, vol. 27, no. 3, pp. 1620–1628, Jul. 2012.

[30] J. Cao, W. Du, H. Wang, and S. Bu, "Minimization of transmission loss in meshed AC/DC grids with VSC-MTDC networks," *IEEE Trans. Power Syst.*, vol. 28, no. 3, pp. 3047–3055, 2013.

[31] W. Zhao, Z. Zhang, and L. Wang, "Manta ray foraging optimization: An effective bio-inspired optimizer for engineering applications," *Eng. Appl. Artif. Intell.*, vol. 87, Jan. 2020, Art. no. 103300, doi: 10.1016/j.engappai.2019.103300.

[32] S. I. Selem, H. M. Hasanien, and A. A. El-Fergany, "Parameters extraction of PEMFC's model using manta rays foraging optimizer," *Int. J. Energy Res.*, vol. 44, no. 6, pp. 4629–4640, May 2020, doi: 10.1002/er.5244.

[33] A. M. Shaheen, R. A. El-Sehiemy, and S. M. Farrag, "A reactive power planning procedure considering iterative identification of VAR candidate buses," *Neural Comput. Appl.*, vol. 31, no. 3, pp. 653–674, Mar. 2019.

[34] A. M. Shaheen, R. A. El-Sehiemy, and S. M. Farrag, "A novel adequate bi-level reactive power planning strategy," *Int. J. Electr. Power Energy Syst.*, vol. 78, pp. 897–909, Jun. 2016.

[35] J. Beerten, S. Cole, and R. Belmans, "Modeling of multi-terminal VSC HVDC systems with distributed DC voltage control," *IEEE Trans. Power Syst.*, vol. 29, no. 1, pp. 34–42, Jan. 2014.

[36] J. Beerten, S. Cole, and R. Belmans, "Generalized steady-state VSCMTDC model for sequential AC/DC power flow algorithms," *IEEE Trans. Power Syst.*, vol. 27, no. 2, pp. 821–829, May 2012.

[37] A. M. Shaheen and R. A. El-Sehiemy, "A multi-objective salp optimization algorithm for techno-economic based performance enhancement of distribution networks?" *IEEE Syst. J.*, early access, Jan. 27, 2020, doi: 10.1109/JSYST.2020.2964743.

[38] J. Beerten, S. Cole, and R. Belmans, "A sequential AC/DC power flow algorithm for networks containing multi-terminal VSC HVDC systems," in *Proc. IEEE PES General Meeting*, Providence, RI, USA, 2010, pp. 1–7.

[39] Z. Pavić and V. Novoselac, "Notes on TOPSIS method," *Int. J. Res. Eng. Sci.*, vol. 1, no. 2, pp. 5–12, 2013.

[40] A. M. Shaheen, S. M. Farrag, and R. A. El-Sehiemy, "MOPF solution methodology," *IET Gener., Transmiss. Distrib.*, vol. 11, no. 2, pp. 570–581, Jan. 2017.

[41] A. M. Shaheen, R. A. El-Sehiemy, and S. M. Farrag, "Solving multi-objective optimal power flow problem via forced initialised differential evolution algorithm," *IET Gener., Transmiss. Distrib.*, vol. 10, no. 7, pp. 1634–1647, May 2016.

[42] M. Rezaei Adaryani and A. Karami, "Artificial bee colony algorithm for solving multi-objective optimal power flow problem," *Int. J. Electr. Power Energy Syst.*, vol. 53, pp. 219–230, Dec. 2013.

[43] M. Ghasemi, S. Ghavidel, M. Gitizadeh, and E. Akbari, "An improved teaching–learning-based optimization algorithm using Lévy mutation strategy for non-smooth optimal power flow," *Int. J. Electr. Power Energy Syst.*, vol. 65, pp. 375–384, Feb. 2015.

[44] S. Duman, "Symbiotic organisms search algorithm for optimal power flow problem based on valve-point effect and prohibited zones," *Neural Comput. Appl.*, vol. 28, no. 11, pp. 3571–3585, Nov. 2017.

[45] A.-A.-A. Mohamed, Y. S. Mohamed, A. A. M. El-Gaafary, and A. M. Hemeida, "Optimal power flow using moth swarm algorithm," *Electr. Power Syst. Res.*, vol. 142, pp. 190–206, Jan. 2017.

[46] M. Abdo, S. Kamel, M. Ebeed, J. Yu, and F. Jurado, "Solving non-smooth optimal power flow problems using a developed grey wolf optimizer," *Energies*, vol. 11, no. 7, p. 1692, Jun. 2018.

[47] M. A. Taher, S. Kamel, F. Jurado, and M. Ebeed, "An improved moth-flame optimization algorithm for solving optimal power flow problem," *Int. Trans. Electr. Energy Syst.*, vol. 29, no. 3, p. e2743, Mar. 2019.

[48] A. Alhejji, M. E. Hussein, S. Kamel, and S. Alyami, "Optimal power flow solution with an embedded center-node unified power flow controller using an adaptive grasshopper optimization algorithm," *IEEE Access*, vol. 8, pp. 119020–119037, 2020.

[49] H. Pulluri, R. Naresh, and V. Sharma, "A solution network based on stud krill herd algorithm for optimal power flow problems," *Soft Comput.*, vol. 22, no. 1, pp. 159–176, Jan. 2018.

[50] A. Ramesh Kumar and L. Premalatha, "Optimal power flow for a deregulated power system using adaptive real coded biogeography-based optimization," *Int. J. Electr. Power Energy Syst.*, vol. 73, pp. 393–399, Dec. 2015.

[51] A. Shabanpour-Haghighi, A. R. Seifi, and T. Niknam, "A modi-fied teaching–learning based optimization for multi-objective optimal power flow problem," *Energy Convers. Manage.*, vol. 77, pp. 597–607, Jan. 2014.

[52] A. M. Shaheen and R. El-Sehiemy, "Optimal co-ordinated al-location of distributed generation units/capacitor banks/voltage regulators by EGWA," *IEEE Syst. J.*, early access, May 6, 2020, doi: 10.1109/JSYST.2020.2986647.

[53] A. M. Shaheen and R. A. El-Sehiemy, "Application of multi-verse opti-mizer for transmission network expansion planning in power systems," in *Proc. Int. Conf. Innov. Trends Comput. Eng. (ITCE)*, Aswan, Egypt, 2019, pp. 371–376, doi: 10.1109/ITCE.2019.8646329.

[54] S. Mirjalili, "Dragonfly algorithm: A new meta-heuristic optimization technique for solving single-objective, discrete, and multi-objective prob-lems," *Neural Comput. Appl.*, vol. 27, no. 4, pp. 1053–1073, May 2016.

[55] A. Askarzadeh, "A novel Metaheuristic method for solving constrained engineering optimization problems: Crow search algorithm," *Comput. Struct.*, vol. 169, pp. 1–12, Jun. 2016.

[56] A. M. Shaheen and R. A. El-Sehiemy, "Optimal allocation of capac-itor devices on MV distribution networks using crow search algo-rithm," *CIRED–Open Access Proc. J.*, vol. 2017, no. 1, pp. 2453–2457, Oct. 2017.

[57] D. K. Sambariya and R. Prasad, "Robust tuning of power system sta-bilizer for small signal stability enhancement using metaheuristic bat algorithm," *Int. J. Electr. Power Energy Syst.*, vol. 61, pp. 229–238, Oct. 2014.

[58] E. S. Ali, "Optimization of power system stabilizers using BAT search algorithm," *Int. J. Electr. Power Energy Syst.*, vol. 61, pp. 683–690, Oct. 2014.

[59] A. Faramarzi, M. Heidarinejad, S. Mirjalili, and A. H. Gandomi, "Marine predators algorithm: A nature-inspired Metaheuristic," *Expert Syst. Appl.*, vol. 152, Aug. 2020, Art. no. 113377, doi: 10.1016/j.eswa.2020.113377.

• • •